

SILVER SEPP

Influence of porosity of the
carbide-derived carbon on the
properties of the composite
electrocatalysts and characteristics
of polymer electrolyte fuel cells



SILVER SEPP

Influence of porosity of the
carbide-derived carbon on the
properties of the composite
electrocatalysts and characteristics
of polymer electrolyte fuel cells



Institute of Chemistry, Faculty of Science and Technology, University of Tartu,
Estonia

Dissertation is accepted for the commencement of the degree of Doctor of
Philosophy in Chemistry on December 12th, 2016 by the Council of the Institute
of Chemistry, University of Tartu.

Supervisor: Prof. Enn Lust, University of Tartu, Estonia
Ph.D. Jaak Nerut, University of Tartu, Estonia

Opponent: Prof. Pawel J. Kulesza
Department of Chemistry, University of Warsaw, Poland

Commencement: January 19th, 2017 at 13.15. 14a Ravila Str., Tartu
(Chemicum), auditorium 1021

Publication of this dissertation is granted by University of Tartu, Estonia.



ISSN 1406-0299
ISBN 978-9949-77-323-7 (print)
ISBN 978-9949-77-324-4 (pdf)

Copyright: Silver Sepp, 2017

University of Tartu Press
www.tyk.ee

TABLE OF CONTENTS

| | |
|--|----|
| 1. LIST OF ORIGINAL PUBLICATIONS | 7 |
| 2. ABBREVIATIONS AND SYMBOLS | 8 |
| 3. INTRODUCTION..... | 11 |
| 4. LITERATURE OVERVIEW | 12 |
| 4.1 Fuel Cells..... | 12 |
| 4.2 Support materials for PEMFC electrodes..... | 15 |
| 4.2.1 Expectations and variety of possible supports | 15 |
| 4.2.2 Carbide-derived carbon | 16 |
| 4.3 Oxygen electroreduction reaction at fuel cell cathode | 17 |
| 4.4 Methods for physical characterization of materials..... | 19 |
| 4.4.1 Gas sorption for porosity characterization | 19 |
| 4.4.1.1 Brunauer-Emmett-Teller theory | 20 |
| 4.4.1.2 Calculation of the total pore volume | 21 |
| 4.4.1.3 The <i>t</i> -plot method | 21 |
| 4.4.1.4 The non-local density functional theory..... | 21 |
| 4.4.2 X-ray diffraction..... | 22 |
| 4.5 Electrochemical characterization methods | 23 |
| 4.5.1 Cyclic voltammetry | 23 |
| 4.5.1.1 Electrochemically active surface area of platinum catalyst..... | 24 |
| 4.5.2 Rotating disk electrode method..... | 25 |
| 4.5.3 Electrochemical impedance spectroscopy..... | 26 |
| 4.6 Performance characteristics of a fuel cell..... | 27 |
| 5. EXPERIMENTAL | 30 |
| 5.1 Synthesis of carbide-derived carbon powders | 30 |
| 5.2 Preparation of Pt-nanoclusters activated catalysts..... | 30 |
| 5.3 Structural characterization of catalysts, catalyst supports and single cell electrodes..... | 31 |
| 5.4 Preparation of catalyst ink and electrodes | 31 |
| 5.5 Electrochemical measurements | 32 |
| 5.5.1 Experiments in a three-electrode glass cell | 32 |
| 5.5.2 PEMFC single cell experiments..... | 33 |
| 6. RESULTS AND DISCUSSION | 34 |
| 6.1 Physical characteristics of the materials..... | 34 |
| 6.2 Electrochemical characterization of carbon and Pt-C materials on glassy carbon electrodes | 39 |
| 6.3 Electrochemical characterization of Pt-C(Mo ₂ C) electrodes in PEM single cells..... | 42 |
| 6.3.1 The polarization and power density curves..... | 42 |
| 6.3.2 CV and EIS data for single cells studied..... | 45 |
| 6.3.3 Time stability tests | 47 |

| | |
|-----------------------------|-----|
| 7. SUMMMARY..... | 49 |
| 8. REFERENCES..... | 50 |
| 9. SUMMARY IN ESTONIAN..... | 56 |
| 10. ACKNOWLEDGEMENTS..... | 58 |
| PUBLICATIONS..... | 59 |
| CURRICULUM VITAE..... | 124 |
| ELULOOKIRJELDUS..... | 127 |

1. LIST OF ORIGINAL PUBLICATIONS

- I **S. Sepp**, E. Härk, P.Valk, K. Vaarmets, J. Nerut, R. Jäger, E. Lust, Impact of the Pt catalyst on the oxygen electroreduction reaction kinetics on various carbon supports, *Journal of Solid State Electrochemistry*, 18 (5) (2014) 1223–1229.
- II **S. Sepp**, J. Nerut, K. Vaarmets, R. Kanarbik, I. Tallo, H. Kurig, E. Lust, The Impact of Pt-nanocluster Deposition and Nafion® Content on the Oxygen Electroreduction Kinetics on Molybdenum Carbide Derived Carbon Synthesized at 1000°C, *ECS Transactions* 61 (2014) 37–50.
- III **S. Sepp**, K. Vaarmets, J. Nerut, I. Tallo, E. Tee, H. Kurig; J. Aruväli, R. Kanarbik, E. Lust, Performance of Polymer Electrolyte Membrane Fuel Cell Single Cells Prepared Using Hierarchical Microporous-Mesoporous Carbon Supported Pt Nanoparticles Activated Catalysts, *Electrochimica Acta*, 203 (2016) 221–229.
- IV **S. Sepp**, J. Nerut, K. Vaarmets, R. Kanarbik, I. Tallo, H. Kurig, E. Lust, Enhanced Stability of Novel Hierarchical Carbon Supports in PEMFC Application, *ECS Transactions*, 75 (14) (2016) 789–799.
- V **S. Sepp**, K. Vaarmets, J. Nerut, I. Tallo, E. Tee, H. Kurig; J. Aruväli, R. Kanarbik, E. Lust, Enhanced Stability of Symmetrical Polymer Electrolyte Membrane Fuel Cell Single Cells Based on Novel Hierarchical Microporous-Mesoporous Carbon Supports, *Journal of Solid State Electrochemistry*, (2016) DOI: 10.1007/s10008-016-3448-4.

Author's contribution

- Paper I: The author performed the electrochemical measurements. The author participated in the analysis of data and preparation of manuscript.
- Paper II: The author performed the electrochemical measurements. The author is mainly responsible for analysis of data and preparation of manuscript.
- Paper III: The author performed the electrochemical measurements. The author is mainly responsible for analysis of data and preparation of manuscript.
- Paper IV: The author performed the electrochemical measurements. The author is mainly responsible for analysis of data and preparation of manuscript.
- Paper V: The author performed the electrochemical measurements. The author is mainly responsible for analysis of data and preparation of manuscript.

2. ABBREVIATIONS AND SYMBOLS

ABBREVIATIONS

| | |
|----------------------|--|
| ac | alternating current |
| AFC | alkaline fuel cell |
| BET | Brunauer-Emmett-Teller |
| C(Mo ₂ C) | carbon synthesized from Mo ₂ C |
| C(WC) | carbon synthesized from WC |
| CDC | carbide-derived carbon |
| CNT | carbon nanotube |
| CV | cyclic voltammetry method |
| CVs | cyclic voltammograms |
| dc | direct current |
| DAFC | direct alcohol fuel cell |
| DCFC | direct carbon fuel cell |
| DMFC | direct methanol fuel cell |
| ECA | electrochemically active surface area |
| EIS | electrochemical impedance spectroscopy |
| FC | fuel cell |
| GCDE | glassy carbon disk electrode |
| GDL | gas diffusion layer |
| HRSEM | high resolution scanning electron microscopy |
| HRTEM | high resolution transmission electron microscopy |
| HSAG | high surface area graphite |
| MCFC | molten carbonate fuel cell |
| MEA | membrane electrode assembly |
| NLDFT | non-local density functional theory |
| OCP | open circuit potential |
| ORR | oxygen electroreduction reaction |
| PAFC | phosphoric acid fuel cell |
| PEMFC | polymer electrolyte membrane fuel cell |
| RDE | rotating disk electrode |
| RH | relative humidity |
| RHE | reversible hydrogen electrode |
| rms | root-mean-square |
| rpm | revolutions per minute |
| SEM | scanning electron microscopy |
| SHE | standard hydrogen electrode |
| SOFC | solid oxide fuel cell |
| wt% | weight percentage |
| TEM | transmission electron microscopy |
| TGA | thermogravimetric analysis |
| XRD | X-ray diffraction |

ROMAN SYMBOLS

| | |
|--------------------|--|
| a | lattice parameter from XRD data |
| A_{CS} | molecular cross-section area of adsorbate (0.162 nm^2 for N_2 at 77 K) |
| c | constant in BET theory describing the adsorbent-adsorbate interactions |
| $c_{\text{O}_2}^b$ | concentration of O_2 in the bulk solution ($1.13 \times 10^{-6} \text{ mol cm}^{-3}$ in 0.5 M H_2SO_4 at 25 °C) |
| C | capacitance |
| C_{CV} | capacitance calculated from CV data |
| C_d | differential capacitance of electrical double layer |
| C_p | parallel capacitance |
| C_s | series capacitance |
| c_f | O_2 concentration in the Nafion [®] film |
| d | Pt crystallite size calculated by Scherrer method (Pt(220) reflection) from XRD data |
| D_f | O_2 diffusion coefficient in the Nafion [®] film |
| D_{O_2} | diffusion coefficient for O_2 in the bulk solution ($1.8 \times 10^{-5} \text{ cm}^2 \text{ s}^{-1}$ in 0.5 M H_2SO_4 at 25 °C) |
| E_0 | amplitude of the sinusoidal voltage |
| E | potential |
| ΔE | potential difference |
| E_p | peak potential |
| f | frequency |
| F | Faraday constant (96490 C mol^{-1}) |
| I | current |
| i | imaginary unit $i = \sqrt{-1}$ |
| I_0 | amplitude of the sinusoidal current |
| I_C | capacitive current |
| I_f | faradaic current |
| I_p | peak current |
| j | current density |
| j_D | diffusion step limited charge transfer current density |
| j_f | current density in the Nafion [®] film |
| j_K | kinetic current density |
| K | constant in the Scherrer equation ($K = 0.93$) |
| k_{het} | electrochemical rate constant for ORR |
| L_f | thickness of Nafion [®] film |
| M | molar mass |
| m_{ad} | mass of adsorbent |
| m_{Pt} | mass of platinum |
| n | number of electrons transferred |
| N_A | Avogadro constant ($6.022 \cdot 10^{23}$ molecules per mole) |
| O | oxidized species |

| | |
|--------------|---|
| P | pressure |
| P/P_0 | relative pressure |
| Q_{DL} | calculated charge for double layer formation |
| Q_H | calculated charge required for hydrogen adsorption at the Pt-nanoparticle surface |
| $Q_{H, ref}$ | charge required to oxidize a monolayer of hydrogen atoms at flat polycrystalline Pt surface (0.21 mC cm^{-2}) |
| Q_{tot} | calculated total charge transferred within the hydrogen adsorption/desorption potential region |
| R | ideal gas constant ($8.314 \text{ J mol}^{-1} \text{ K}^{-1}$) |
| R | reduced species |
| R_P | parallel resistance |
| R_S | series resistance |
| S_{BET} | specific surface area |
| S_{ext} | external surface area |
| S_{meso} | mesoporous area |
| S_{micro} | microporous area |
| t | time |
| T | temperature |
| t_{stat} | statistical thickness of the adsorbed layer |
| V_{ads} | volume of adsorbate |
| V_{meso} | mesoporous volume |
| V_{micro} | microporous volume |
| V_{molar} | molar volume of adsorbate ($34.7 \text{ cm}^3 \text{ mol}^{-1}$ for N_2 at 77 K) |
| V_{tot} | total pore volume |
| W | mass of gas adsorbed at relative pressure |
| W | pore width |
| W_m | mass of gas absorbed in monolayer |
| Z | impedance |
| $ Z $ | magnitude of impedance |
| Z' | real part of the impedance |
| Z'' | imaginary part of the impedance |

GREEK SYMBOLS

| | |
|-----------|---|
| β | the full width at half maximum |
| ϕ | phase difference between voltage and current |
| θ | Bragg angle |
| λ | wavelength |
| ω | angular frequency |
| v | potential scan rate |
| ν | kinematic viscosity of the solution ($0.01 \text{ cm}^2 \text{ s}^{-1}$ for H_2O at $20 \text{ }^\circ\text{C}$) |

3. INTRODUCTION

Polymer electrolyte membrane fuel cells (PEMFCs) are regarded as a promising alternative energy conversion devices for both mobile and stationary applications [1–4]. These environmentally clean cells generate water, heat, and electricity via an electrochemical reaction with hydrogen as a fuel and oxygen in the air as an oxidant [1–6]. Due to relatively high efficiency, low operating temperature and quick start-up time, PEMFCs are mostly used in automotive applications and in residential co-generation systems [1–4]. Main problem hindering the wide-scale commercialization of PEMFCs is high overpotential for oxygen electroreduction reaction (ORR) at the porous cathode decreasing the efficiency of the fuel cell. Therefore, novel materials are being sought for PEMFC applications [5–7].

Platinum is the most common catalyst material used for PEMFC electrodes. Apart from Pt, some other precious metals alloys with high stability have been investigated as alternatives to Pt in fuel cells [8,9]. Various precious metal free electrocatalysts have also been studied, but insufficient electrochemical stability is the main problem hindering the commercial application of these materials.

The efficiency and stability of a electrocatalyst depends strongly on the selection of an appropriate support material. The demands for support material are suitable porosity for quick mass transport, high electrical conductivity and electrochemical stability [1–4,10]. Carbon is the most widely used support material for PEMFC catalysts because of its affordability, suitable porosity, high electrical conductivity and relatively high electrochemical stability [10].

The properties of the carbon support have significant impact on the PEMFC performance and the structure of catalyst layer should be carefully optimized in order to achieve further improvement in the fuel cell performance [10–12]. Corrosion of carbon support for conventional cathode catalysts is a critical problem for PEMFC durability under start-stop conditions in automotive applications [13–15]. Therefore different carbon supports have been tested during long-term catalyst optimization studies for quick start-up of PEMFC [13–17].

Carbon materials can be synthesized using various methods like the high temperature carbonization of carbon rich organic precursors which is the most widely utilized method [15]. In order to prepare carbon powders with very high specific surface area, selective extraction of non-carbon elements from carbides have been used [18–21]. Resulting carbide-derived carbons (CDCs) are unique materials in which the pore size, shape and other parameters can be controlled in a very exact manner [18,19,21]. It has been suggested that CDCs are viable fuel cell catalyst supports that are capable of realizing the full activity of Pt nanoparticles with superior corrosion stability [21–24].

CDCs with well-defined properties are excellent objects to study the impact of carbon electrocatalyst support properties on the performance of a PEMFC. The main aim of this work was to study the suitability of the Pt nanoclusters activated CDCs in the fuel cell application and to compare the properties of these materials with commonly used commercial carbon support Vulcan XC72.

4. LITERATURE OVERVIEW

4.1 Fuel Cells

Fuel cell (FC) is an electrochemical device that converts chemical energy directly into electrical energy and some dissipative heat. The intermediate step of producing mechanical work is avoided. The efficiency of FCs is high, because unlike thermal external or internal combustion engines, there are no thermodynamic limitations of Carnot cycle. Depending on the chemical composition of the fuel and oxidant on which the FC is operated, different products can be generated. A traditional hydrogen-oxygen FC generates only water as the by-product. Possible fuels beside hydrogen are gaseous hydrocarbons (e.g. CH₄), alcohols (e.g. CH₃OH, C₂H₅OH) and other hydrogen rich organic compounds or mixtures. Oxygen from air is mostly used as an oxidant. FCs generate electricity without involving any moving parts and with minimal generation of noise and pollutants [25–27].

In 1838 Sir William Robert Grove experimented with electrochemically cleaned platinum wires, mineral-acid electrolytes and voltaic piles. As one upper half on Pt wire was exposed to hydrogen gas and the other to oxygen gas, galvanometer indicated the flow of electricity [25]. At the same time Cristian Friedrich Schönbein recognized that it was caused by the electrochemical action between Pt wires and two gases applied. Today we refer to it as the first H₂-O₂ FC. During 1890s and the following decades, galvanic cells received full recognition as highly efficient energy conversion devices. In 1894 W.F. Ostwald provided basic theoretical understandings of how FC operates realizing that it could be more efficient energy conversion device than combustion engine, which is limited by the efficiency of Carnot cycle [25,27].

The first practical FC was developed by English engineer F.T. Bacon, who started working on FCs in 1932 and completed the construction of 5 kW FC stack in 1952 [27]. In early 1960s FC technology reached a turning point when NASA decided to develop alkaline FC for the Apollo space modules [25]. Subsequent milestone in FC technology included the development of chemically resistant perfluorinated proton exchange membranes, such as Nafion[®], and the use of Nafion[®]-containing FC electrodes incorporating high-surface area Pt nanoparticles on catalyst support rather than low-surface-area Pt-black. Driven by automotive industry, PEMFCs have been receiving increased attention since the early 1990s as an alternative power source for vehicles [25,26,28].

The most common classification of FCs is based on the type of electrolyte used in the cells and includes [28]:

- 1) polymer electrolyte membrane fuel cell,
- 2) alkaline fuel cell (AFC),
- 3) phosphoric acid fuel cell (PAFC),
- 4) molten carbonate fuel cell (MCFC), and
- 5) solid oxide fuel cell (SOFC).

The choice of electrolyte dictates the operating temperature range of the FC. The operating temperature and useful life of a FC determine the physicochemical and thermomechanical properties of materials used as the cell components (i.e., electrodes, electrolyte, interconnect, current collector, etc.) [28]. Depending on the electrolyte and temperature, different fuels and catalysts can or must be employed (Table 1). While hydrogen or a liquid organic compounds are the fuels for low-temperature FCs, high-temperature FCs can be operated using wider range of fuels, including low molecular weight hydrocarbons or CO-contaminated feeds [25].

Table 1. Summary of major differences of the fuel cells [29].

| | PEMFC | AFC | PAFC | MCFC | SOFC |
|-------------------------------------|--|--|------------------------|---|--|
| Electrolyte | Hydrated polymer ion exchange membrane | Potassium Hydroxide in asbestos matrix | Phosphoric Acid in SiC | Liquid Molten Carbonate in LiAlO_2 | Perovskites (Ceramics) |
| Electrode matrix/ catalyst supports | Carbon | Transition metals | Carbon | Nickel and Nickel Oxide | Perovskite and perovskite / metal cermet |
| Catalyst | Platinum | Platinum | Platinum | Electrode material | Electrode material |
| Operating temperature | 40–80 °C | 65–220 °C | 205 °C | 650 °C | 600–1000 °C |
| Interconnect | Carbon or metal | Metal | Graphite | Stainless steel or nickel | Nickel, ceramic or steel |
| Charge carriers | H^+ | OH^- | H^+ | CO_3^{2-} | O^{2-} |
| Prime cell component | Carbon-based | Carbon-based | Graphite-based | Stainless-based | Ceramic |

In parallel with the classification by electrolyte, some FCs are classified by the type of fuel used, e.g. direct alcohol fuel cell (DAFC) or direct carbon fuel cell (DCFC). DAFC (more commonly direct methanol fuel cell or DMFC) refers to PEMFC-type FC, where methanol or another alcohol is used as fuel without external reforming. In DCFC, solid carbon powder is used as fuel in anode without gasification step. Concepts with solid oxide, molten carbonate, and alkaline electrolytes are all under intensive development [28]. Alkaline membrane fuel cells are also under development, but highly conducting solid alkaline membrane has remained elusive to date [25].

Fig. 1 depicts schematically the structure of hydrogen FC device with proton conducting membrane (i.e. PEMFC). In this electrochemical cell the overall reaction can be separated to two half-cell reactions: molecular hydrogen is oxidized at the anode and the resulting protons move through the membrane and react with oxygen to form water on the cathode. At the same time electrons move from anode to cathode through external electric circuit.

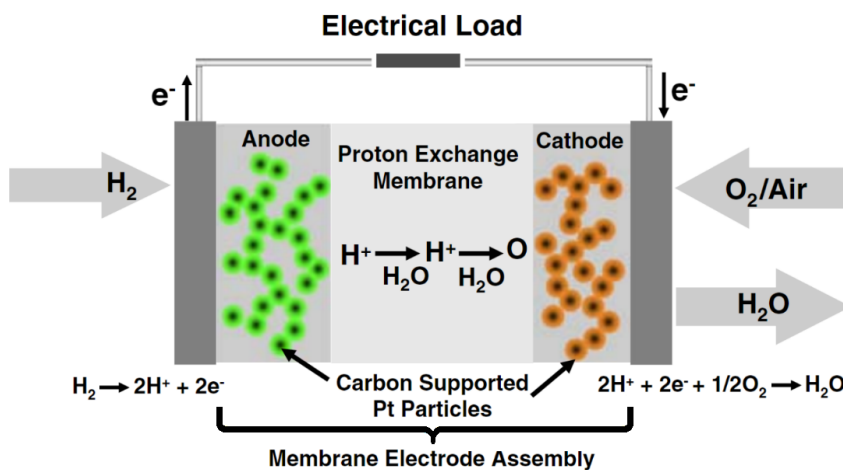


Figure 1. Working principle scheme of H₂-O₂ fuel cell [30].

A PEMFC consists of two electrodes in contact with an electrolyte membrane (Fig. 1). The membrane is designed as an electronic insulator that separates the reactants and allows only the transport of ions and water. The electrodes are constituted of a porous gas diffusion layer (GDL) and a catalyst (usually platinum supported on high surface area carbon) containing active layer. This membrane electrode assembly (MEA) is sandwiched between two electrically conducting bipolar plates with integrated gas distribution channels [31]. The electrodes host the electrochemical reactions within the catalyst layer and provide electronic conductivity, and pathways for reactant supply to the catalyst and removal of products from the catalyst.

The GDL is a carbon paper or cloth that provides rigidity and support to the MEA. It incorporates hydrophobic material (e.g. Teflon[®]) that facilitates the product water drainage and prevents the gas paths from flooding. The active layer consists of catalyst particles, ionomer and pore spaces which form a three-phase boundary where the electrochemical reaction takes place. Electrochemical oxidation of hydrogen and reduction of oxygen can only occur at interfacial boundary regions, where gas molecules reach catalyst surfaces that are connected electrically to the external circuit through a conducting support (usually carbon) and are accessible to the proton-conducting medium (Nafion[®]) [30]. A good electrode has to effectively facilitate the trade-off between enabling

high catalytic activity, retaining enough water to guarantee good proton conductivity in the ionomer phase, and having an optimal pore size distribution to facilitate rapid gas transport. All the components of the MEA need to be stable (under both chemical and mechanical stresses) for several thousands of hours in the FC under the operating conditions [28,31].

The main advantages of a PEMFC are: high fuel conversion efficiency (34–36%), rapid start-up due to low operating temperature, capability to generate high current and power densities, relatively long life, no moving parts and therefore quiet operation. Although, there are many significant future challenges in PEMFC design and development such as carbon corrosion, catalyst deactivation, thermal and water management and sensitivity to poisoning by CO and oxygen containing intermediates, sulphur containing components/species and NH₃. Finally, hydrogen infrastructure needs great investments, being economical barrier for development and commercialization of PEMFC based technologies [25,27,28,32].

4.2 Support materials for PEMFC electrodes

4.2.1 Expectations and variety of possible supports

In PEMFC application highly dispersed Pt or Pt-based catalysts on a conductive support are commonly used as electrodes for hydrogen electrooxidation and ORR [33]. In such catalysts, the high surface area to volume ratio maximizes the area available for reactions [26]. The efficiency of a catalyst depends strongly on the selection of an appropriate support material. The main demands for a support material are high surface area to obtain high metal dispersion, suitable porosity (so-called open porosity) for quick mass transport, high electrical conductivity and electrochemical stability (i.e. voltage cyclability) [1–3, 14,26,34–36]. Various catalyst supports have been studied and discussed by Antolini et al. [15,36]. Carbon blacks are manufactured by the pyrolysis of hydrocarbons such as natural gas or oil fractions from petroleum processing. Due to its low cost and high availability, oil-furnace carbon black (e.g. Vulcan XC72) has been used widely as the support for platinum catalyst. High surface area graphite (HSAG) can be prepared from graphitized material by a special grinding process. Surface areas of 100–300 m²g⁻¹ make this graphite an interesting support material for precious metal clusters based catalysts [37]. Carbon nanotubes (CNTs), nanofibers, carbon gels, boron doped diamond and ordered mesoporous carbons have been studied as electrocatalyst supports as well [15,26]. The stability towards carbon oxidation/reduction process, known as carbon corrosion, is the major problem regarding their use in PEMFC application [1,38,39]. The corrosion originates from the thermodynamic instability of carbon under the conditions of the PEMFC cathode as carbon can be oxidized to CO₂ according to the net reaction:



This process may be accelerated by the presence of Pt and by exposing the electrode to high potentials, which occur during FC start-up and shutdown via the so-called “reverse-current decay mechanism” [38].

To avoid carbon corrosion several ceramic materials have been investigated as catalyst supports [10]. Electrically conductive sub-stoichiometric metal oxides (e.g. Ti_2O_7 and Ebonex) and doped metal oxides such as doped TiO_2 and SnO_2 , nanostructured metal oxides, such as TiO_2 nanotubes and WO_2 nanorods, metallic conductor RuO_2 and d-metal carbides (e.g. WC) have been proposed as corrosion resistant catalyst supports. Although these materials have demonstrated high electrochemical stability and the ability to act as co-catalyst, all ceramic materials mentioned have low specific surface area and low or only acceptable electron conductivity hindering their application as a catalyst support in PEMFC. The Pt nanoparticles have been also dispersed into polyaniline and other conducting polymer (e.g. polypyrrole, polythiophene) matrixes. However, the loss of electronic conductivity in the potential range for ORR is the major problem limiting their application as electrocatalyst supports for PEMFCs [26]. Therefore, carbon materials, including porous carbon powders, are the most widely utilized supports due to suitable electronic conductivity and porosity granting high dispersion of Pt nanoparticles [1,17].

Chai et al. [14], Antolini et al. [15,36] and Uchida et al. [11,12] have demonstrated that the properties of the carbon support have significant impact on the PEMFC performance and the structure of the catalyst layer should be carefully optimized in order to achieve further improvement in the cathode performance. Uchida et al. concluded that the influence of the carbon supports on PEMFC performance is remarkable, indicating that carbon support is the key material in PEMFC [12].

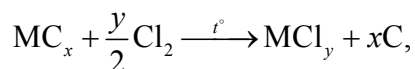
It has been reported that carbon materials with both high surface area and good crystallinity can not only provide a high dispersion of Pt nanoparticles, but also facilitate electron transfer, resulting in better device performance [15]. Under start-stop conditions the corrosion (oxidation/reduction) of carbon support for conventional cathode catalysts is a critical problem for PEMFC durability in automotive applications due to the elevated electrode potentials [10,13–15,35,36]. Influence of structural parameters of PEMFC electrodes like the particle size, inter-particle distance and metal loading have been systematically tested and summarized in many papers [10–15,35,36,40]. The challenge is to develop carbon supports with high surface area, good electrical conductivity, suitable porosity to allow good reactant flux to catalytic centres, and high electrochemical stability in fuel cell environment. Synthesis methods under studies and applications should be relatively simple and not too expensive [15]

4.2.2 Carbide-derived carbon

Well-defined hierarchical porous carbon materials with high specific surface area and bimodal pore size distribution can be prepared using the selective extr-

action of non-carbon elements from metal and non-metal binary and ternary carbides [19–21,23,24,41–45]. High-temperature etching in halogen gas (e.g. chlorine) is prevalent synthesis method of carbide-derived carbons (CDCs). However, leaching in supercritical water, high temperature decomposition and vacuum decomposition can be used as well [46].

Usually CDCs are synthesized via chlorination process according to following reaction:



where M is carbide forming element (e.g. Mo, W, Ti, Si, V, Cr, Fe, B, Al). Additional oxidation process with water vapour or CO₂ can be applied to open the closed pores of carbon material prepared [41,45,47]. This is followed by high-temperature treatment with H₂ or H₂ mixture with inert gas during a few hours to remove residual chlorine and oxygen containing functional groups from the carbon surface [18,41,43].

Resulting CDCs are unique micro- and mesoporous materials with controlled graphitization level, size and shape of pores, ratio of micropore area to mesopore area, ratio of micropore volume to mesopore volume etc. Thus, different important parameters can be controlled in a very exact manner [19–24,41–45]. Various tunable hierarchical porous structures can be synthesized using different precursors (Mo₂C, WC, TiC, SiC etc.) and thermal treatment conditions. It has been suggested that CDCs are viable fuel cell catalyst supports that are capable of realizing the full potential and electrochemical activity of carbon supported Pt nanoparticles with superior corrosion stability [16,17,20–24].

4.3 Oxygen electroreduction reaction at fuel cell cathode

The main problem hindering the wide-scale commercialization of PEMFCs is high overpotential for oxygen electroreduction at the cathode, determining the efficiency of the FC. The identification of the mechanistic sluggishness and irreversibility of the ORR has been major challenge for decades [25]. The mechanism and kinetics of the ORR at cathode depend on many parameters, of which the most important are the chemical composition of the cathode and the electrode potential applied.

Carbon supported platinum is commonly used as anode and cathode catalyst in PEMFCs. The need to modify the characteristics of the catalyst has emerged due to several factors, such as reducing the price of the active catalyst and increasing its activity, selectivity, and long-term stability.

Novel materials prepared are usually first tested in a three-electrode cell on glassy carbon electrode as these experiments are less expensive and complex than the two-electrode experiments in completed single cells. Rotating disk electrode (RDE) and rotating ring disk electrode methods allow establishment

of the electrochemical activity of catalyst materials and determination of some reaction intermediates. Therefore, using these methods reaction mechanism of ORR can be proposed. In acidic aqueous solution the reaction can proceed through two plus two electron transfer pathway via H_2O_2 intermediate. It was determined that the two electron pathway reaction takes place on pure carbon support [48]:



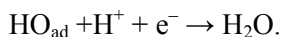
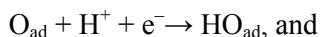
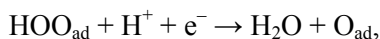
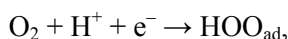
However, electroreduction of H_2O_2 may also take place in solution or in FC:



For FC, the more preferred reaction pathway is the four-electron transfer reaction. This is the expected pathway on Pt-nanoclusters activated carbon electrodes:



Pt is the most active and time-stable catalyst for ORR and therefore most commonly used metal catalyst in PEMFC [50]. Marković et al. [51] studied ORR on the different crystallographic orientations of Pt electrode surface in 0.1 M HClO_4 solution. They found that the activity for ORR decreases in the order: $\text{Pt}(110) > \text{Pt}(111) > \text{Pt}(100)$. For all low-index Pt planes the Tafel-plot slopes were found to be -120 mV dec^{-1} at high current densities and -60 mV dec^{-1} at low current densities. It was proposed that oxygenated surface intermediates chemisorbed on Pt are the cause of the change in the Tafel-plot slope value [51]. The four-electron ORR, which is predominant in PEMFC with Pt catalyst, consists of several elementary steps involving number of oxygenated surface intermediates. One of the proposed mechanisms has been obtained using DFT-based calculations [52]:



The surface intermediates reduce the rate of ORR and in the case of Pt the electrochemical reaction is limited by too strong bond of adsorbed HO_{ad} [52]. The four-electron pathway is preferred in PEMFC, because H_2O_2 can oxidize carbon

support and proton conducting membrane reducing the time stability of FC materials. It is assumed that if ORR takes place on pure carbon support with different number of edge planes, the reaction can proceed via both pathways depending on the exact location of the reaction site. In that case the number of electrons transferred in the reaction (calculated using Koutecky-Levich equation) varies within the range from two to four. [17,21,23]. Compton et al. studied ORR in acid solution on several carbon materials including basal plane pyrolytic graphite and edge plane pyrolytic graphite [53]. They concluded that, within these graphitic structures, the substrates with a large number of edge plane sites have a higher activity towards ORR and therefore a higher tendency to produce H_2O_2 if used as a catalyst support in a PEMFC. It is therefore favourable to decrease the number of edge plane sites in carbon catalyst supports for PEMFC in order to reduce possible membrane and support degradation caused by H_2O_2 attack [53].

As CDCs can be synthesized with various tunable properties, it is possible to tailor the suitable support material for ORR [16,21]. Schlange et al. used TiC based CDCs as supports at DMFC cathode achieving 18% higher power density values compared with those for carbon black (Vulcan XC72R) supported catalysts [54]. They related improved performance with the inhomogeneous catalysts dispersion, a higher surface area of CDC support, the smaller platinum particles sizes compared to carbon black supported catalyst and the more graphitic ordering of TiC–CDC reducing the electric resistance [55]. RDE data for various CDCs indicate, that Mo_2C based carbon materials with variable physical properties are interesting and promising objects to be used as catalyst supports for PEMFC. [20,21,24]

4.4 Methods for physical characterization of materials

The composition and structure of FC catalyst and/or support have a significant influence on the performance, stability and cost of FC. Significant efforts have been made to obtain the structural information of the materials used in FCs and to link this information with the measured electrochemical data, in order to successfully design and optimize the electrode surface and porous structure [26].

4.4.1 Gas sorption for porosity characterization

Gas sorption is one of the important and informative experimental methods employed for the characterization of the porous materials. Combined N_2 and CO_2 adsorption data at 77 K and 273 K are mainly used to characterize mesopores of carbon materials. It allows to access wide range of pore sizes, from 0.35 to 100 nm [56]. According to IUPAC nomenclature, pores can be classified according to the diameter (W): pores with $W < 2$ nm are micropores, mesopores diameter is within the range from 2 nm to 50 nm and macropores are larger than 50 nm [46,57].

4.4.1.1 Brunauer-Emmett-Teller theory

The Brunauer-Emmett-Teller (BET) adsorption theory is widely used for calculation of the specific surface area of catalyst and various other finely divided powders and porous materials [58–61]. The BET equation is given as:

$$\frac{1}{W\left(\frac{P}{P_0}-1\right)} = \frac{1}{W_m c} + \frac{c-1}{W_m c} \cdot \frac{P}{P_0} \quad (1)$$

where W is the mass of gas adsorbed at relative pressure P/P_0 , W_m is the mass of adsorbate in a monolayer. BET constant c is related to the adsorption energy of the adsorbed monolayer, i.e. it describes the adsorbent-adsorbate interactions. Thus, the BET plot (adsorption isotherm) in coordinates $1/\{W[(P/P_0)-1]\}$ vs. P/P_0 should be linear. However, for many materials the linearity is achieved within the P/P_0 range from 0.05 to 0.35. The mass of adsorbate can be calculated from the slope and intercept of the BET plot (2):

$$\text{slope} = \frac{c-1}{W_m c} \quad (2)$$

$$\text{intercept} = \frac{1}{W_m c} \quad (3)$$

$$W_m = \frac{1}{\text{slope} + \text{intercept}} \quad (4)$$

The specific surface area, S_{BET} , can be calculated using the W_m value by following equation:

$$S_{\text{BET}} = \frac{W_m N_A A_{\text{CS}}}{M m_{\text{ad}}} \quad (5)$$

where N_A is the Avogadro constant ($6.022 \cdot 10^{23}$ molecules per mole), A_{CS} is the molecular cross-section area of adsorbate (0.162 nm^2 for N_2 at 77 K [60,61]), M is the molar mass of adsorbate (28 g mol^{-1} for N_2) and m_{ad} is the adsorbent mass i.e. mass of the sample.

4.4.1.2 Calculation of the total pore volume

The total pore volume, V_{tot} , is defined as the liquid volume absorbed at certain relative pressure, when the sorption isotherm exhibits a distinct plateau. In this case, it is assumed that all pores are filled with liquid adsorbate and thus, the density of the adsorbate is equal to the density of the liquid bulk at saturation pressure [59,62]. At pressure P and temperature T , the total pore volume V_{tot} can be calculated using the following equation:

$$V_{\text{tot}} = \frac{PV_{\text{ads}}V_{\text{molar}}}{RT}, \quad (6)$$

where V_{ads} is the volume of adsorbate adsorbed, V_{molar} is the molar volume of adsorbate ($34.7 \text{ cm}^3 \text{ mol}^{-1}$ for N_2 at 77 K) and R is the ideal gas constant ($8.314 \text{ J mol}^{-1} \text{ K}^{-1}$).

4.4.1.3 The t -plot method

The t -plot method extends to higher relative pressures compared to the BET method and therefore enables determination of the so-called external surface area S_{ext} of the adsorbent material, i.e. meso- and macroporous surface area [62,63]. The adsorbed gas volume V_{ads} is plotted against the statistical thickness of the adsorbed layer t_{stat} to obtain the so-called t -plot. A convenient method to calculate t_{stat} has been proposed by de Boer et al. [64]:

$$t_{\text{stat}} = \sqrt{\frac{13.99}{\log \frac{P}{P_0} + 0.034}}. \quad (7)$$

The S_{ext} value can be calculated from the slope of the linear high-pressure area of the t -plot and the intercept extrapolated to the volume axis will provide the micropore volume (V_{micro}). The surface area of micropores, S_{micro} , can be found from the difference of total surface area and meso- and macropore area:

$$S_{\text{micro}} = S_{\text{BET}} - S_{\text{ext}}. \quad (8)$$

4.4.1.4 The non-local density functional theory

One of the most accurate methods to describe pore size distribution of microporous-mesoporous materials is the non-local density functional theory (NLDFT) [65]. To practically apply this approach for the calculation of the pore

size distribution from the experimental adsorption isotherms, theoretical model isotherms have to be calculated using methods of statistical mechanics [56]. NLDFT describes objectively the local structure of the condensed adsorbate at the curved solid surfaces. The shape of the isotherm is determined by the intermolecular forces between liquid-liquid and liquid-solid interfaces. Generalized adsorption isotherm describes relation between isotherm shape and molecular forces:

$$N\left(\frac{P}{P_0}\right) = \int_{W_{\min}}^{W_{\max}} N\left(\frac{P}{P_0}, W\right) f(W) dW, \quad (9)$$

where $N(P/P_0)$ is the experimental adsorption isotherm data point, W is the pore width and $f(W)$ is the pore size distribution function. It is assumed that the final isotherm consists of many individual isotherms of single pores multiplied by their distribution function $f(W)$ over the range of pore sizes expressed in porous structure [65,66].

4.4.2 X-ray diffraction

X-ray powder diffraction (XRD) is a rapid analytical technique allowing qualitative and quantitative identification of the structure of the crystalline compound. The studied solid sample is mounted into a goniometer and illuminated with a finely focused monochromatic X-ray beam, producing a diffraction pattern. Information about the arrangement and the spacing of atoms in crystalline materials can be determined studying the XRD diffraction pattern characteristics, which are unique for each crystalline substance. Thus, if an exact match can be found between the reference pattern and the sample under study, the chemical and crystallographic identity can be assumed and thus verified. [67,68]

XRD allows determination of the crystallite size of Pt catalyst used in PEMFC electrodes. The Lorentzian band shape and the Gaussian error-distribution function are usually used for approximation of the band shape with a meaningful mathematical function. The crystallite size d can be calculated by the Scherrer equation:

$$d = \frac{K \lambda}{\beta \cos \theta}, \quad (10)$$

where K is a dimensionless shape factor ($K = 0.93$), λ is the X-rays wavelength of the beam used, β is the full width at half maximum of the reflections and θ is the Bragg angle [69].

4.5 Electrochemical characterization methods

4.5.1 Cyclic voltammetry

Cyclic voltammetry (CV) is a potentiodynamic method in which a continuously cycling potential is applied across the electrode-electrolyte interface and the resulting current is measured. In the CV method the electrode potential is changed with fixed rate from the initial potential to the final potential and then inverted back to the initial potential. The corresponding relationship between applied potential and measured current is called cyclic voltammogram [26,70].

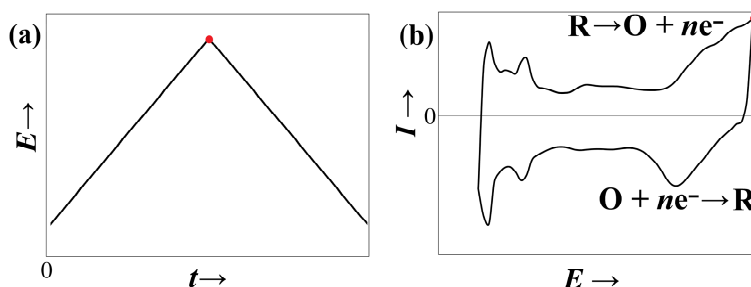


Figure 2. (a) Cyclic potential sweep and (b) resulting cyclic voltammogram if reversible oxidation/reduction process occurs.

In the case of a reversible electron transfer (reduction) reaction of the type $O + ne^- \rightarrow R$ (O is the oxidized form and R is the reduced form of an electrochemically active substance), an inverse peak appears in the reverse scan of cyclic voltammogram (Figure 2). The rate of the heterogeneous electron transfer and/or homogeneous chemical process accompanying electrochemical charge transfer step could be determined based on the measurement of peak potential, E_p , and peak current, I_p , data as a function of electrode potential scan rate, v .

It has been demonstrated that the CV can be used for describing the reversibility of different redox processes by analysis of the difference between oxidation and reduction E_p -values. The difference between corresponding peaks is $58/n$ mV for a reversible process of n electrons transfer. In the case of partially reversible process, the distance between the peaks is wider and peak current values change. If the reaction is irreversible (e.g. ORR), no inverse peaks appear in the reverse potential scan [70].

The total current measured (Eq. 11) is the sum of the faradaic current (I_f) which is caused by the electrochemical reaction, and capacitive current (I_C) contribution. I_C is caused by the double layer charging or discharging while scanning the electrode potential. Ideally, the value of capacitive current is linear function of the electrode potential scan rate.

$$I = I_C + I_f = C_d \frac{dE}{dt} + I_f = \nu C_d + I_f, \quad (11)$$

where C_d is the differential capacitance of the electrical double layer. These contributions can be subtracted by analysing the cyclic voltammograms (CVs) measured in several values of ν .

If current is proportional to ν ($I_C \propto \nu$) then the adsorption step limits the process and if I_f is proportional to square root of ν ($I_f \propto \nu^{1/2}$) then it is a mass transfer limited process [70].

4.5.1.1 Electrochemically active surface area of platinum catalyst

The most widely used application of *CV* to PEMFCs is the determination of electrochemically active surface area (ECA) of the Pt-based electrocatalysts [26]. In aqueous electrolyte or in MEA, when potential of Pt-based electrocatalyst is cycled within the range from 0 to 1.2 V vs RHE, the current peaks caused by adsorption/desorption of hydrogen adatoms on the surface of Pt appear within the potential range from 0 to 0.4 V. [26,71] In potential range from 0.7 to 1.2 V the current peaks are caused by Pt oxidation in the so-called forward and Pt oxide reduction in the reverse scan (towards negative potentials).

However, the ECA value is determined from current peaks of the H adatoms adsorption/desorption (or proton reduction/hydrogen ionization). The charge values, Q_H , for corresponding processes can be calculated applying the following equation:

$$Q_H = Q_{\text{total}} - Q_{\text{DL}}, \quad (12)$$

where Q_{total} is the charge transferred within the hydrogen adsorption/desorption potential region and Q_{DL} is the charge for double layer formation which has been estimated through a linear extrapolation of the capacitance value from the so-called double layer region (approximately from 0.4 V). The ECA for Pt (in $\text{m}^2 \text{g}^{-1}$) can be calculated with respect to the mass of Pt from the following formula:

$$\text{ECA} = \frac{Q_H}{m_{\text{Pt}} \cdot Q_{\text{H,ref}}}, \quad (13)$$

where m_{Pt} is the mass of Pt deposited onto/into the electrode (mg) and $Q_{\text{H,ref}}$ is the charge required to oxidize a monolayer of hydrogen atoms H_{ad} or to reduce H_3O^+ forming the monolayer of H_{ads} on the compact polycrystalline (metallic) Pt (assumed as 0.21 mC cm^{-2}) [71,72].

4.5.2 Rotating disk electrode method

The most common method for analysis of the electrochemical activity of newly-developed catalysts is the rotating disk electrode (RDE) method in aqueous electrolyte. This technique allows relatively quick determination of the ORR activity of the catalyst studied and it can be to some extent connected with the activity of the catalyst in MEA, as long as the weight of catalyst is precisely known [26].

In the RDE method it is assumed that the rate of mass transport to the porous and rough electrode surface is uniform. The other important assumption is that the flow rate of the solution around electrode is laminar in case of all rotation rates. If the flow is laminar, it is possible to calculate the rate of mass transport applying the theory developed by Levich [70]:

$$j_D = -0.62nFD_{O_2}^{2/3}v^{-1/6}\omega^{1/2}c_{O_2}^b, \quad (14)$$

where j_D is the diffusion step limited charge transfer current density, n is the number of electrons transferred per electroreduction of one O_2 molecule, F is the Faraday constant, D_{O_2} is the diffusion coefficient for O_2 ($1.8 \times 10^{-5} \text{ cm}^2 \text{ s}^{-1}$ in 0.5 M H_2SO_4 at 25 °C [13]), $c_{O_2}^b$ is the concentration of O_2 in the bulk solution ($1.13 \times 10^{-6} \text{ mol cm}^{-3}$ in 0.5 M H_2SO_4 at 25 °C [73]), v is the kinematic viscosity of the aqueous solution ($0.01 \text{ cm}^2 \text{ s}^{-1}$ [13]), ω is the angular velocity of the rotating electrode. Based on the Levich equation, the limiting current depends linearly on the reagent concentration. Thus, Eq. 14 can be used to calculate the diffusion coefficient for reacting species in solution. In addition, Eq. 14 can be used for calculation of the number of electrons (n) if the charge transfer rate is limited by the diffusion.

In the mixed kinetics control region, the Koutecky-Levich equation [74–76] can be applied:

$$\frac{1}{j} = \frac{1}{j_K} + \frac{1}{j_D} = -\frac{1}{nFk_{\text{het}}c_{O_2}^b} - \frac{1}{B\omega^{1/2}}, \quad (15)$$

where j_K is the kinetic current density, k_{het} is the electrochemical rate constant for ORR and $B = 0.62nFD_{O_2}^{2/3}v^{-1/6}c_{O_2}^b$. From the slope value of the linear Koutecky-Levich plot ($1/j$ vs $1/\omega^{1/2}$), the diffusion coefficient or the number of electrons transferred can be calculated. Most importantly, from the intercept the kinetic current densities can be calculated [74–76].

The RDE data for supported catalyst with relatively thick catalyst layer can be analyzed using the so-called two active layers model, which takes into account the diffusion in the electrolyte boundary-layer and in Nafion film [77,78]:

$$\frac{1}{j} = \frac{1}{j_K} + \frac{1}{j_D} + \frac{1}{j_f} = -\frac{1}{nFk_{\text{het}}c_{\text{O}_2}^b} - \frac{1}{B\omega^{1/2}} - \frac{L_f}{nFc_fD_f}, \quad (16)$$

where j_f is the current density in the Nafion[®] film with thickness L_f , c_f and D_f are the O_2 concentration and diffusion constant in the Nafion[®] film, respectively. However, analysis made by Behm et al. [79,77] demonstrated that for thin Pt-carbon film electrodes ($L_f < 0.1 \mu\text{m}$) the role of Nafion[®] layer was unimportant (if $j_f \gg j_k$) and thus the classical Koutecky-Levich equation can be applied.

4.5.3 Electrochemical impedance spectroscopy

Electrochemical impedance spectroscopy (EIS) is technique, where a small alternating current (ac) voltage or current with controlled amplitude and frequency is added to the direct current (dc) signal and is applied to the electrochemical cell. The amplitude and phase of the resulting signal, current if controlling voltage or vice versa, are measured with respect to those of the perturbation signal. This is repeated over a wide range of frequencies to obtain an impedance spectrum. Mathematical and physical analysis of the signal provides the extent of influence of resistance (R), capacitance (C) and inductance on the processes occurring at a specific frequency [70,80]. EIS enables separate evaluation of series resistance, overall resistance and any faradaic resistance caused by the electrochemical reactions. In case of PEMFC materials, EIS is used to study ORR kinetics, mass transport losses, evaluate ohmic resistance and electrode properties such as double layer capacitance [26].

If a monochromatic alternating voltage $E(t) = E_0\sin(\omega t)$ is applied to an electrode, then the resulting current is $I(t) = I_0\sin(\omega t + \phi)$, where ϕ is the phase difference between the voltage and the current (depending on the physical characteristics of the system) and E_0 and I_0 are the amplitudes of the sinusoidal voltage and current, respectively. Based on the Ohm's law, the complex resistance (impedance), Z , is defined as, [70,74,76]:

$$Z = \frac{E(t)}{I(t)} = |Z|e^{i\phi} = Z' + iZ'' \quad (17)$$

with $i = \sqrt{-1}$, where Z' and Z'' are the real and imaginary parts of the impedance. The impedance of the real electrochemical system is a function of frequency.

For an ideal resistor, the phase shift is zero ($\phi = 0$) and for an ideal capacitor $\phi = -\pi/2$ rad. For a real electrochemical interphase the phase shift depends on the electrochemical processes taking place at the interface and thus on the frequency and potential applied.

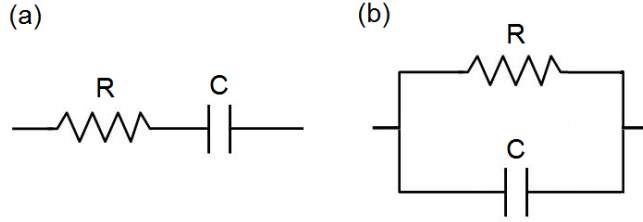


Figure 3. Equivalent RC circuits, where resistance and capacitance are connected (a) in series and (b) in parallel.

In Figure 3(a) the resistor and the capacitor are connected in series (so called series RC circuit) and the following relations are valid:

$$Z' = R_s \text{ and } C_s = -\frac{1}{Z'' \cdot \omega}, \quad (18)$$

where R_s and C_s are the series resistance and series capacitance. In Figure 3(b) the corresponding elements are connected in parallel, and the following relations are valid:

$$\frac{|Z|^2}{Z'} = R_p \text{ and } C_p = -\frac{Z''}{|Z|^2 \cdot \omega}, \quad (19)$$

where R_p and C_p are the parallel resistance and parallel capacitance. $|Z| = \sqrt{(Z')^2 + (Z'')^2}$ is the magnitude of impedance. For an ideally polarizable interface the series and the parallel capacitances are overlapping [70,76].

4.6 Performance characteristics of a fuel cell

The theoretical, thermodynamic reversible cell voltage of a H₂-O₂ FC at open circuit potential (OCP) (i.e at zero current condition) and standard conditions is $E^0 = 1.23$ V. Upon current flow, a number of voltage losses occur in FC decreasing the cell voltage according to Eq. 20 [25]:

$$\Delta E = E^0 - \eta_{\text{act, cathode}} - \eta_{\text{act, anode}} - iR_{\text{ohmic}} - \eta_{\text{conc, cathode}} - \eta_{\text{conc, anode}}. \quad (20)$$

Thus, the voltage loss is caused by activation losses (faradaic reactions activation energies) at the cathode and anode ($\eta_{\text{act, cathode}}$ and $\eta_{\text{act, anode}}$), ohmic drop across the membrane and external circuit caused by the combined electronic, ionic and contact resistance, R_{ohmic} , and concentration overpotentials at both

electrodes ($\eta_{\text{conc, cathode}}$ and $\eta_{\text{conc, anode}}$), which become noticeable or rate limiting at higher current densities, were large amount of fuel and oxidant react at anode and cathode.

Fig. 4 illustrates how the ideal cell voltage (without any losses) differs from real FC behaviour. Activation overvoltages are the largest cause of loss of voltage and hence the efficiency of a FC. This is why great deal of research has been and will be focused on the discovery of improved FC electrocatalysts.

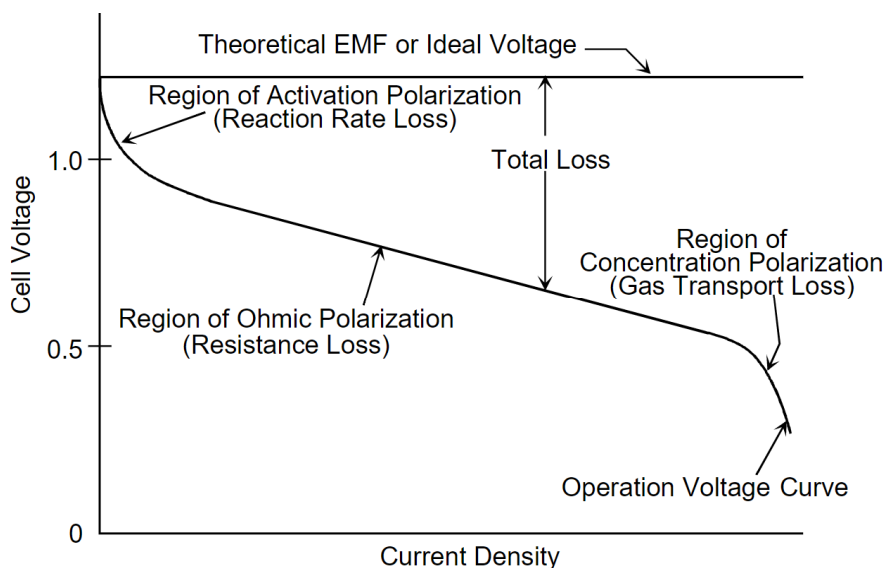


Figure 4. Ideal and actual $\text{H}_2\text{-O}_2$ FC voltage/current curve [29].

Activation loss is caused by the activation overvoltages at cathode and anode for ORR and hydrogen electrooxidation reaction, respectively. Typically, $\eta_{\text{act, cathode}}$ exceeds $\eta_{\text{act, anode}}$ by at least two magnitude. This is why improved ORR electrocatalyst offers much larger gain in FC voltage and hence, efficiency. Therefore much more effort is directed toward development of more efficient electrocatalyst materials for ORR [25,27].

Besides the efficiency, the stability of electrocatalyst materials is also extremely important. During operation, a PEMFC exhibits a gradual decline in power output as individual components are exposed to an aggressive combination of strong oxidizing conditions like low pH, high temperature, high water content and high electrochemical potential and oxygen concentration [39,81]. Various degradation mechanisms cause decay of PEMFC performance during operation [82]. At least four possible mechanisms have been proposed to describe the decay of Pt-based catalyst: [30]:

- 1) growth of Pt-nanoparticles via Ostwald ripening,
- 2) detachment of Pt-nanoparticles from the support,

- 3) dissolution and re-precipitation of Pt-nanoparticles in the ion conductor, and
- 4) coalescence of of Pt-nanoparticles by migration on the support.

The dominant mechanism of decay depends on the operational conditions of PEMFC and the type of catalyst material used. Under ideal PEMFC operational conditions (from 0.6 V to OCP) Pt dissolution and PtO formation and subsequent chemical dissolution are both possible mechanisms of Pt area loss. During FC start-stop conditions, where cathode potential can reach up to +1.5 V, carbon oxidation/reduction (corrosion) is the main reason of catalyst degradation [26]. At lower electrode potential values, carbon corrosion to CO₂ can be also enhanced by Pt catalysts, which may cause permanent loss of support material and even the collapse of the electrode [39,81]

5. EXPERIMENTAL

5.1 Synthesis of carbide-derived carbon powders

Catalyst supports were synthesized from carbides using the chlorination method at different fixed temperatures from 600 to 1100 °C [19,42–44]. The starting materials were Cl₂ (99.999%, AGA), tungsten carbide (α -WC, 99%, particle size <10 μ m, Aldrich), and molybdenum carbide (Mo₂C, 99.5%, –325 mesh powder, Sigma-Aldrich). The chlorination temperature for WC was 1100 °C and for Mo₂C within the range from 600 to 1000 °C, selected to prepare carbon materials with a wide variation of porosity and crystallinity characteristics [42–45]. Carbide was loaded into a quartz vessel in a tube furnace and it was reacted with Cl₂ for 6 h at a flow rate of 50 ml min⁻¹. After chlorination, the reactor was flushed with a stream of Ar (99.9999%, AGA) to remove the excess of chlorine and residues of gaseous and adsorbed by-products from the nanoporous carbon surface formed. Additional cleaning, i.e treatment with H₂/Ar (1:4) mixture was performed at 800 °C for 2 h to remove the residual chlorine, chlorides, and oxygen-containing functional groups from the surface of porous CDC powder. The corresponding carbide-derived carbons are noted below as: C(Mo₂C)600 °C, C(Mo₂C)750 °C, C(Mo₂C)800 °C, C(Mo₂C)850 °C, C(Mo₂C)900 °C, C(Mo₂C)1000 °C and C(WC) 1100 °C [16,17,42,43].

5.2 Preparation of Pt-nanoclusters activated catalysts

The Pt nanoparticles were deposited onto carbon supports by the so-called sodium borohydride reduction method [14,23,33,40,83]. The required quantity of H₂PtCl₆×6H₂O (99.9 %, Alfa Aesar) was dissolved in Milli-Q+ water, and the mixture was diluted to prepare a solution with a total Pt concentration of ~2 mM. The solution was thereafter stirred at ambient temperature for 1 h. The pH of the solution was adjusted to ~8 with dropwise addition of 20 wt% NaOH (99.99 %, Sigma-Aldrich) solution. The required amount of carbon powder was suspended in Milli-Q+ water and stirred to form a homogeneous carbon slurry, which was added into an aqueous solution of H₂PtCl₆. Thereafter, the NaBH₄ (\geq 98.0 %, Aldrich) was dissolved in Milli-Q+ water and the prepared solution was added carefully to the previously prepared carbon suspension. The reaction mixture received was stirred for 2 h and left to settle overnight. The catalyst was filtered, rinsed with Milli-Q+ water, and dried in a vacuum oven at 80 °C. The amount of Pt in all the catalysts prepared was ~70 wt % (14 at%). The prepared catalysts will be noted as Pt-C(Mo₂C)600 °C, Pt-C(Mo₂C)750 °C, Pt-C(Mo₂C)800 °C, Pt-C(Mo₂C)850 °C, Pt-C(Mo₂C)900 °C, Pt-C(Mo₂C)1000 °C, Pt-C(WC)1100 °C, and Pt-C(Vulcan).

5.3 Structural characterization of catalysts, catalyst supports and single cell electrodes

The XRD patterns for the materials were collected with a Bruker D8 Advance diffractometer with Ni filtered CuK_α radiation (0.6 mm wide parallel beam, two 2.5° Soller slits and LynxEye line detector). The scanning step of 0.01° for 2θ was applied from 16° to 90° and the total counting time per step was 166 s. The X-ray tube was operated at 40 kV and 40 mA.

The thermogravimetric analysis (TGA) in the atmosphere consisting of 80 vol% N_2 and 20 vol% O_2 was carried out in order to estimate the content of Pt in the catalyst materials using NETZSCH STA449F3. The temperature was varied from 40 to 1000 $^\circ\text{C}$ with a heating rate of 5 $^\circ\text{C}/\text{min}$ and with gas flow rate of $120 \text{ cm}^3 \text{ min}^{-1}$. Weight of the samples tested in the Al_2O_3 pan was 7–9 mg.

The porosity of the powders was estimated using the low-temperature ($-195.8 \text{ }^\circ\text{C}$) nitrogen sorption method [66] combined with CO_2 sorption method [84] (Micromeritics ASAP 2020). The non-local density functional theory and the slit shape pore model [14,84] were used for the pore size distribution calculation. The values of specific surface area were calculated using the Brunauer-Emmett-Teller multipoint theory [66] within the relative pressure (p/p_0) range from 0.05 to 0.2. The total volume of pores (near saturation pressure) and the volume of micropores were calculated using the t -plot method assuming the Harkins and Jura thicknesses between 0.5 and 0.9 nm [61].

The high-resolution transmission electron microscopy (HRTEM) images were measured on a Tecnai 12 instrument, operated at a 120 kV accelerating voltage [85]. HRTEM studies were conducted in Aalto University. The high-resolution scanning electron microscopy (HRSEM) data were obtained using HeliosTM Nanolab 600. The cross-sectional views of MEAs were studied using Microtrac Semtrac system.

5.4 Preparation of catalyst ink and electrodes

Catalyst ink was prepared by suspending the Pt-C powder in the solution of Milli-Q⁺ water, isopropanol (Sigma-Aldrich, >99%) and Nafion[®] dispersion (Aldrich) in such ratio that the final dry catalyst layer would have 5 wt% content of Nafion[®] in the electrodes deposited onto glassy carbon disk electrode (GCDE) support and 20–25 wt% content of Nafion[®] ionomer in the single cell electrodes. Ink was agitated in an ultrasonic bath for 30 min to wet and disperse the catalyst and Nafion[®] thoroughly and homogeneously.

In the experiments with three-electrode configuration, glassy carbon disk electrodes (GCDEs) (diameter 5 mm), pressed into a Teflon[®] holder, were used [17,20,21,23,24,86,87]. The GCDE was polished with 0.05 μm alumina slurry (Buehler) to a mirror finish. After polishing, the GCDE was washed with Milli-Q⁺ water and sonicated in Milli-Q⁺ water for a few minutes. The catalyst ink was deposited onto the GCDE surface and dried at room temperature. The flat cross-

section surface (geometric) area of the electrode was 0.196 cm^2 . The loading of the Pt-C catalyst on GCDE was approximately 0.5 mg cm^{-2} (thus, $\sim 0.35 \text{ mg Pt}$ per 1 cm^2 geometric surface area). In order to achieve good wetting of the catalyst layer, the electrode was impregnated in Milli-Q⁺ water before the assembling of the electrochemical cell.

In the single cell experiments (two-electrode system) catalyst ink was deposited onto the Nafion[®] 115 membrane using spray gun and dried in vacuum oven at 50 mbar and 80 °C. To avoid the inhomogeneity in the catalyst layer caused by swelling, the MEAs were pressed before and after every coating procedure at 6 MPa in 80 °C using isostatic laminator (Keko ILS-66). The geometric surface area of the electrode was 5 cm^2 . The electrocatalyst loading was $\sim 1.0 \text{ mg cm}^{-2}$, including $\sim 0.7 \text{ mg cm}^{-2}$ Pt in the form of deposited nanoclusters [16].

5.5 Electrochemical measurements

All electrochemical measurements were performed with potentiostat/galvanostat Gamry Reference 600 or Autolab PGSTAT 302 (with Autolab 20A booster for single cell tests).

5.5.1 Experiments in a three-electrode glass cell

Measurements were carried out using a RDE system (Pine Instrumental Company). The counter electrode was a large Pt wire mesh, separated from the main solution by a fritted glass membrane. The working electrode potential was measured against the Hg | Hg₂SO₄ | saturated K₂SO₄ reference electrode, connected to the cell through a long Luggin capillary. Hereafter all potentials are given vs. reversible hydrogen electrode (RHE). The electrodes were submerged in 0.5 M H₂SO₄ (Fluka, TraceSelect[®]Ultra) solution under a standby potential of 1.07 V (vs. RHE), where faradaic current densities were minimal. Thereafter, CVs at different potential scan rates (2 to 200 mV s⁻¹) were collected. After CV measurements, the RDE voltammetry curves were measured at potential scan rate 10 mV s⁻¹ at electrode rotation velocities from 0 to 3000 revolutions per minute (rpm) [20,23,24]. Next, the solution was saturated with high-purity molecular O₂ (99.999 %, AGA), and CVs were measured. The EIS data were obtained in Ar saturated solution at ac frequencies from 0.01 to 10 000 Hz at 0.65 V (vs. RHE) with ac potential modulation of $\pm 5 \text{ mV}$ root mean square (rms). The electrolyte resistance, i.e. the high-frequency series resistance, R_{el} , was calculated from EIS data at $f \rightarrow \infty$ ($R_{el} = Z' (f \rightarrow \infty)$), and it was used to correct the measured electrode potentials against ohmic potential (iR) drop in the solution phase between the electrode and the tip of the Luggin capillary in the three-electrode system. All measurements were carried out at temperature $22 \pm 1 \text{ }^\circ\text{C}$, and at least four different electrodes, prepared using identical conditions, were tested [17,20,23,24,87].

5.5.2 PEMFC single cell experiments

The MEA prepared was placed between the graphite plates with septrine gas flow channels. Teflon[®] gaskets (0.25 mm) and ELAT 1400W gas diffusion layers were used for assembling the single cell, which was held together by eight 6 mm bolts with a torque of 5 N m [16].

H₂ and O₂ were fed to the anode and cathode at flow rate of 200 cm³ min⁻¹ and 100% relative humidification (100% RH) at temperatures 30, 40, 50 and 60 °C. Gas flow was regulated and humidified using MKS Type M100B mass-flow controllers and a dew point humidification system (Fuel Cell Technologies, Inc.). Polarization and power density curves were measured in the galvanostatic mode. Data were collected with 0.2 A current intervals and each point was measured for 60 s. EIS measurements were performed in galvanostatic (current density $j = 0.4 \text{ A cm}^{-2}$) and potentiostatic (cell potential $\Delta E = 0.55 \text{ V}$) modes at frequency range from 0.5 to 100 000 Hz with an applied ac amplitude of 0.02 A or 0.005 V (rms) respectively.

The ECA was calculated using the traditional hydrogen adsorption method [71] based on the analysis of the current peak areas in the cyclic voltammetry curves (area under the peak is proportional to the charge used for reduction of H₃O⁺ cations) measured within the potential range from 0.04 to 1.1 V vs. RHE at scan rates from 20 to 500 mV s⁻¹ at 30 °C. Humidified (100% RH) N₂ was fed to the cathode and H₂ to the anode with flow rates of 200 cm³ min⁻¹ and 10 cm³ min⁻¹ respectively.

6. RESULTS AND DISCUSSION

6.1 Physical characteristics of the materials

The carbon supports and Pt-C catalyst materials were characterized using several physical methods.

TGA measurements were conducted prior PEM single cell test to determine the exact weight percentage of Pt deposited into/onto catalyst powders prepared. According to the TGA measurement results (Table 2), the platinum content was similar in all the catalyst materials studied [16]. It was established that the average weight percentage of platinum in the samples was 71.8 ± 1.7 . The TGA curves of some Pt-C(Mo₂C) samples are presented in Fig 5. The temperature of carbon burn-off depends somewhat on the graphitization level of the support studied, being in the range from 350 °C to 450 °C.

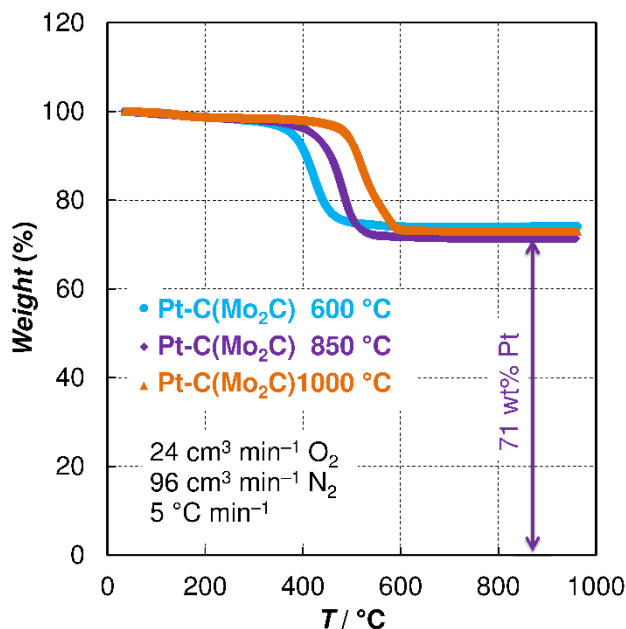


Figure 5. The TGA curves for the Pt-C(Mo₂C) catalysts (noted in figure) in the synthetic air [16].

The collected XRD data are presented in Fig. 6. The diffraction peaks corresponding to the Pt(111), Pt(200), Pt(220), Pt(311) and Pt(222) planes are clearly visible [40]. The average lattice parameter calculated for Pt is 0.3913 ± 0.0001 nm (Table 2) and this value does not depend on the catalyst support used. The average lattice parameter calculated is lower than the lattice

parameter for bulk Pt, but this deviation could be explained by the continuous-medium model [88]. The average crystallite size of the Pt crystallites has been estimated from Pt(220) reflection by using the Scherrer's equation (Eq. 10) [89]. The results of calculations are shown in Table 2. The calculated average crystallite size is 4.5 ± 0.5 nm. The crystallites of platinum deposited onto C(Mo₂C)600 °C and C(Mo₂C)1000 °C supports are slightly bigger, and this is also evident from XRD peaks sharpening shown in Fig. 6. According to the results of the TGA and XRD measurements the reproducibility of the catalyst material characteristics is good.

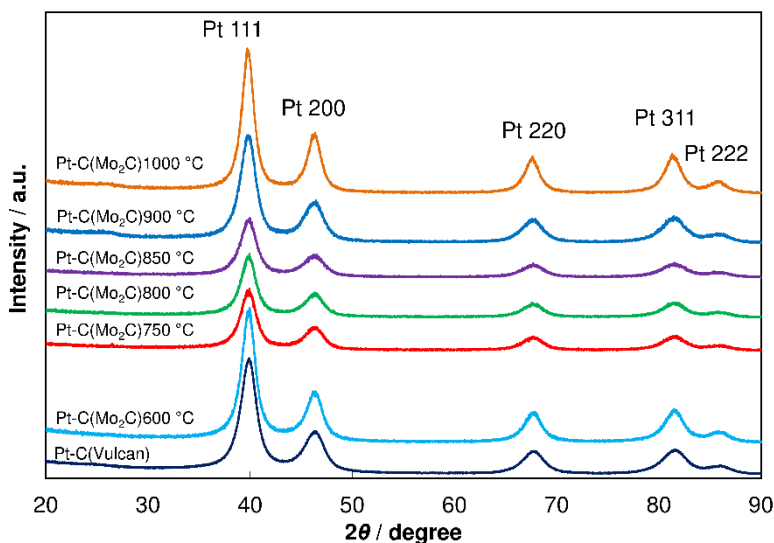


Figure 6. XRD patterns for the Pt-C(Mo₂C) and Pt-C(Vulcan) catalysts synthesized [16].

The results of the N₂ sorption measurements, given in Table 2 indicate that all the catalysts are microporous-mesoporous materials. Generally, S_{BET} increases with the decrease of chlorination temperature (i.e. with the synthesis temperature of the catalyst support C(Mo₂C)). The V_{tot} -value is maximal for Pt-C(Mo₂C)800 °C and the corresponding values for Pt-C(Mo₂C)750 °C and Pt-C(Mo₂C)850 °C are only slightly lower. The same trend has been also followed for unmodified catalyst supports C(Mo₂C) [21].

Fig. 7 presents the pore size distribution data after the Pt nanoparticles deposition onto the carbon supports. All Pt-C(Mo₂C) catalysts have micropores (pores with widths $d \leq 2$ nm) and mesopores ($2 \text{ nm} \leq d \leq 50 \text{ nm}$) [90,91]. However, the materials studied can be divided into three groups based on the pore size distribution data in the region of mesopores. **(A)** Mainly microporous material (Pt-C(Mo₂C)600 °C) with two small peaks in the region of mesopores at 2.9 nm and at 15 nm. **(B)** Microporous-mesoporous materials (Pt-C(Mo₂C)750 °C,

Pt-C(Mo₂C)800 °C and Pt-C(Mo₂C)850 °C) with two well-developed main peaks in the region of mesopores at 3.4 nm and at 15 nm. (C) Microporous-mesoporous materials (Pt-C(Mo₂C)900 °C and Pt-C(Mo₂C)1000 °C) with one peak in the region of mesopores at 8.6 nm. The deposition of the Pt nanoparticles onto C(Mo₂C) does not change the pore size distribution plot shape, i.e. the catalyst and catalyst support have similar microporous-mesoporous structure and comparable pore size distribution [21]. The material Pt-C(Vulcan) has both mesopores and macropores according to pore size distribution plot in Fig. 7 and the pores with size more than 50 nm could be caused by the porosity between the C(Vulcan) particles as the size of the C(Vulcan) particles is about 50-100 nm [16].

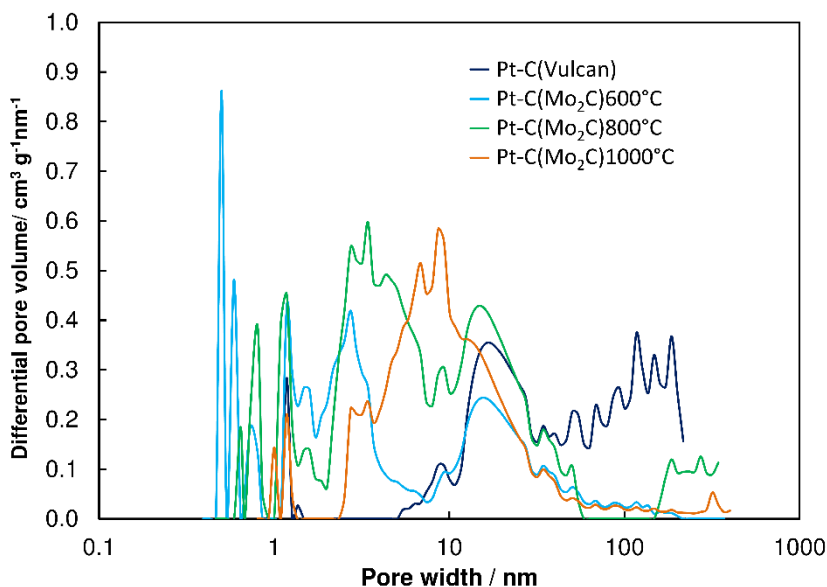


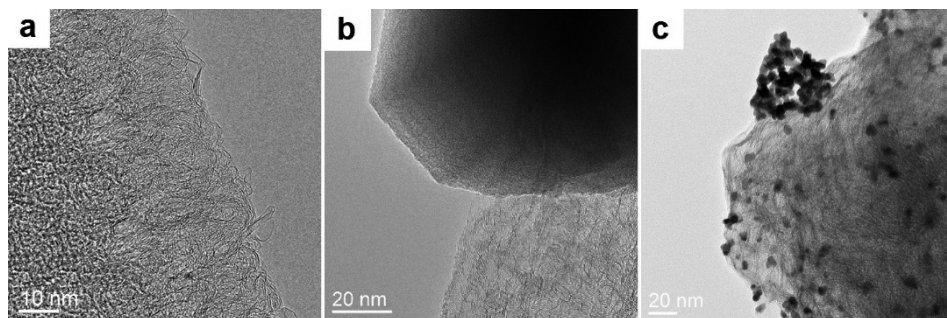
Figure 7. The pore size distribution of the Pt-C(Mo₂C) and Pt-C(Vulcan) catalysts synthesized (noted in figure) [16].

Table 2. Results of N₂ sorption, thermogravimetric and X-ray diffraction measurements [16].

| Catalyst material | $S_{\text{BET}} / \text{m}^2 \text{g}^{-1}$ | $S_{\text{meso}} / \text{m}^2 \text{g}^{-1}$ | $V_{\text{tot}} / \text{cm}^3 \text{g}^{-1}$ | $V_{\text{meso}} / \text{cm}^3 \text{g}^{-1}$ | wt% (Pt) | a (nm) | d (nm) |
|--------------------------------|---|--|--|---|----------|----------|----------|
| Pt-C(Mo ₂ C)600 °C | 510 | 110 | 0.43 | 0.22 | 74 | 0.391 | 4.7 |
| Pt-C(Mo ₂ C)750 °C | 610 | 100 | 0.62 | 0.21 | 70 | 0.391 | 4.1 |
| Pt-C(Mo ₂ C)800 °C | 550 | 200 | 0.64 | 0.41 | 70 | 0.391 | 4.4 |
| Pt-C(Mo ₂ C)850 °C | 450 | 80 | 0.58 | 0.22 | 71 | 0.391 | 4.1 |
| Pt-C(Mo ₂ C)900 °C | 250 | 75 | 0.50 | 0.15 | 74 | 0.391 | 3.8 |
| Pt-C(Mo ₂ C)1000 °C | 220 | 60 | 0.42 | 0.12 | 73 | 0.392 | 5.6 |
| Pt-C(Vulcan) | 94 | 67 | 0.38 | 0.37 | 71 | 0.391 | 4.6 |

S_{BET} – specific surface area; S_{meso} – mesopore area; V_{tot} – total pore volume; V_{meso} – mesopore volume; wt%(Pt) – weight percentage of Pt deposited onto/into the catalyst; a – lattice parameter for Pt; d – crystallite size of Pt calculated using the Scherrer model (based on Pt(220) reflection).

The structure of catalyst materials and carbon supports have been visualized using a HRTEM and HRSEM. Fig. 8a depicts a graphene-like C(WC)1100 °C particle revealing the existence of somewhat ordered graphitic particles in/on the sample surface. On the contrary, Fig 8b shows that other support C(Mo₂C)800 °C is mainly amorphous, presenting only little evidence of interlayer correlation. As it can be seen from Fig 8c, the deposited Pt has formed mainly small and clearly separated nanoparticles ($d < 5$ nm), however some Pt agglomerates have been observed as well.

**Figure 8.** High resolution transmission electron microscopy data for: a) pure carbon support C(WC)1100 °C; b) pure carbon support (Mo₂C)800 °C and c) catalyst material Pt-(Mo₂C)800 °C.

SEM images of MEA prepared from Pt-C(Mo₂C)800 °C are shown in Fig. 9. Electrodes on the both sides of proton conducting Nafion[®] membrane can be

seen in Fig. 9a. The thickness of Pt-C(Mo₂C)800 °C cathode is about 7-10 μm, the thickness of the anode prepared from commercial Pt-C(Vulcan) material is 9-11 μm. The particles of catalyst are clearly visible in Figs 9b and 9c, and a good contact with the electrolyte layer has been achieved.

The size of irregular shaped C(Mo₂C)800 °C particles varies from 1 μm to 4 μm. Large macropores between the Pt-C(Mo₂C)800 °C particles can facilitate the diffusion of reagents and improve water management. The particles of catalyst Pt-C(Vulcan) have a spherical shape with the size about 0.1 μm. The macropores between the Pt-C(Vulcan) particles are of the same order of magnitude (0.1 μm). Fig. 9d demonstrates the HRSEM image of catalyst material Pt- C(Mo₂C)800 °C and it can be seen that the surface of carbon particle has been covered uniformly with the Pt nanoparticles.

The particle size histograms have been constructed for many surface areas and the corresponding data for one selected area is given in Fig. 9d. The average size of the Pt nanoparticle based on the analysis of more than 130 particles is 6.0±1.7 nm. The size of non-agglomerated Pt nanoparticles is statistically reproducible and varies from 5 to 8 nm over wide number of catalysts regions, which is in a good agreement with XRD data (Table 2).

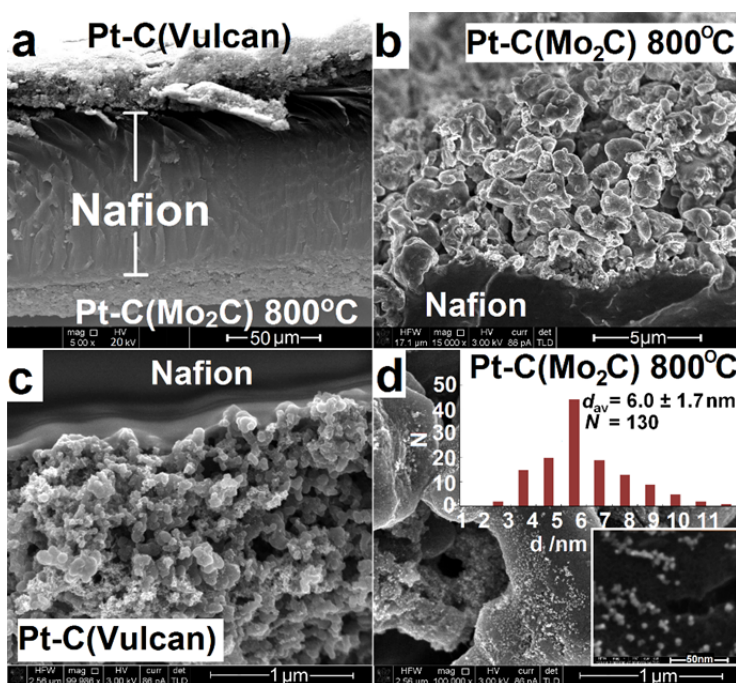


Figure 9. The scanning electron microscopy images a-c): of the membrane electrode assembly (MEA) with cathode: Pt-C(Mo₂C)800 °C and anode Pt-C(Vulcan); d) high resolution scanning electron microscopy image of catalyst Pt-C(Mo₂C)800 °C with histogram for size distribution of Pt nanoparticles.

6.2 Electrochemical characterization of carbon and Pt-C materials on glassy carbon electrodes

Catalyst supports and Pt-nanoclusters activated carbon materials deposited onto GCDE have been tested in 0.5 M H₂SO₄ solution in order to determine their electrochemical activity towards ORR prior to their application in FCs. Different CDCs and Pt-activated catalysts have been studied using RDE, CV and EIS methods and the results have been compared with data for commercial carbon Vulcan and Pt-C(Vulcan) [17,21,85,86].

In paper I [17] two different CDCs are compared with Vulcan XC72R. CV and RDE data show that high cathodic ORR current densities have been achieved for the Pt nanocluster-modified electrodes deposited onto the GCDE support. For Pt-C(Mo₂C) electrode, the overvoltage of ORR is about 0.5 V lower than that for pure catalyst support C(Mo₂C).

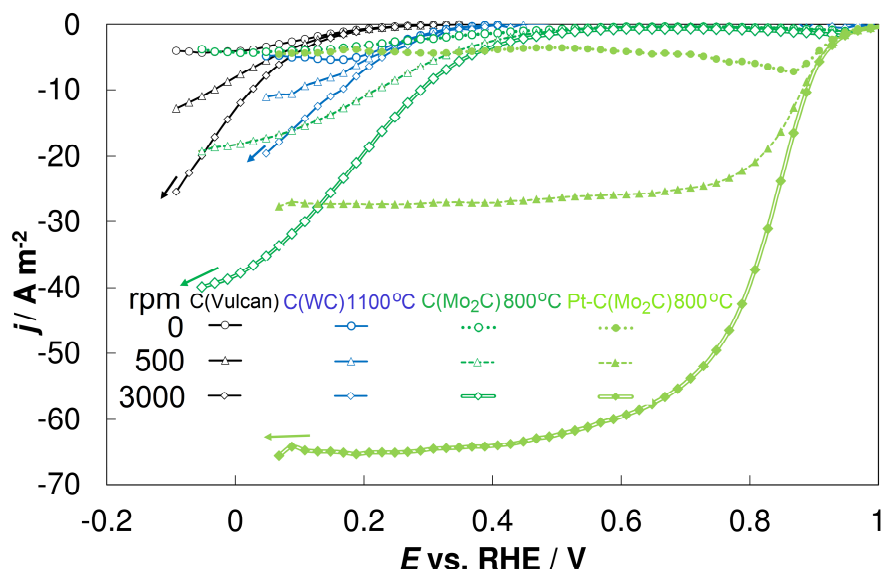


Figure 10. The oxygen reduction current density, j , vs. electrode potential, E , for studied carbide-derived carbons, C(Vulcan) and Pt-C(Mo₂C)800 °C in 0.5 M H₂SO₄ solution at different electrode rotation rates (noted in figure in revolution per minute) given in the figure. Current densities are corrected for current densities in the 0.5 M H₂SO₄ solution, saturated with Ar.

The formation of clear diffusion-limited current plateaus takes place for the ORR on all Pt-nanoclusters activated materials studied. In the case of non-activated C(Mo₂C)800 °C, C(WC)1100 °C or C(Vulcan), the ORR current is only just approaching the plateau region (Fig. 10). The current density values for pure carbon supports are about two times lower than the corresponding values

for Pt-nanoclusters activated carbon materials, because the number of electrons transferred is approximately two or four respectively. It can be seen from Fig. 10 that the electrode overvoltage for ORR decreases in the order $C(\text{Vulcan}) > C(\text{WC})1100^\circ\text{C} > C(\text{Mo}_2\text{C})800^\circ\text{C}$, being nearly 0.3 V lower for $C(\text{Mo}_2\text{C}) 800^\circ\text{C}$ than that for $C(\text{Vulcan})$.

The ORR currents of for the less-ordered $C(\text{Mo}_2\text{C})800^\circ\text{C}$ electrode are higher within the range of studied potentials compared with those for $C(\text{WC})1100^\circ\text{C}$ (Fig. 10). More amorphous $C(\text{Mo}_2\text{C})800^\circ\text{C}$ has more crystallographic defects and edge planes in the structure which are catalytically active centres for the ORR. It has been shown that the current vs. voltage curve for oxygen reduction on the edge plane pyrolytic graphite is shifted by around 0.45 V towards higher positive potentials than that for the $C(0001)$ basal plane [53].

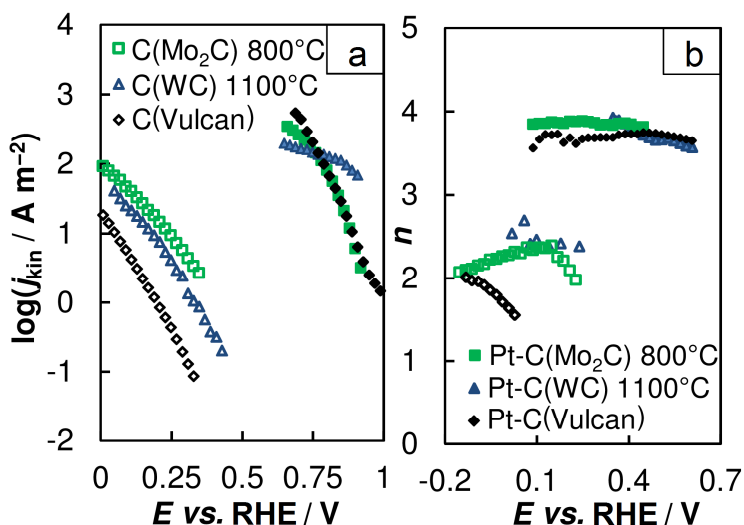


Figure 11. a) Dependence of the logarithm of kinetic current density and b) number of electrons transferred per one oxygen molecule electroreduction vs. electrode potential for non-activated carbon supports (empty markers) and for Pt-C catalysts (filled markers) in 0.5 M H_2SO_4 solution.

Fig. 11 presents the potential dependencies of the logarithm of the ORR kinetic current density and number of electrons transferred for materials studied. The kinetic current densities and number of electrons transferred were calculated using Koutecky–Levich equation (Eq. 15). The numbers of electrons transferred is approximately two for unmodified carbon electrodes being slightly higher for CDCs due to higher number of carbon edge planes. Vulcan XC72R shows approximately one order of magnitude lower kinetic currents (at 0.15 V) than those established for CDCs. It should be noted that if the platinum nanoclusters

are deposited onto the carbon support, the difference in activities of Pt-activated CDCs is still present, indicating that Pt-C(Mo₂C)800 °C has a larger number of catalytic sites and higher dispersion of Pt-nanoparticles. Another reason for the greater activity of C(Mo₂C)800 °C and Pt-C(Mo₂C)800 °C might be the suitable structure of the carbon support, i.e. the more mesoporous C(Mo₂C)800 °C structure facilitates more rapid transport of O₂ molecules within the micro-porous-mesoporous material layer [17,21]. For Pt-modified materials, the number of electrons transferred (calculated within the diffusion-limited potential region) is roughly four and is in good agreement with literature data [34].

In paper II [92] the ORR on the Pt-C(Mo₂C)1000 °C catalyst was studied with different ionomer Nafion[®] mass fractions (from 5 to 30 wt.%). As this carbon material is more graphitized and the specific surface area is lower than that for C(Mo₂C)800 °C, the corresponding electrochemical activity is also lower. It was found that if the content of Nafion[®] increases, the kinetic currents and specific activity of Pt catalyst particles decrease. The same trend was also observed by Koscha et al. [78] and was explained by the mass transport of oxygen in the nanoscale range, electrical resistance caused by coverage of the carbon and Pt with Nafion[®] and by HSO₄⁻ anion adsorption on Pt. Therefore, it has been concluded that the high Nafion[®] content (20-30 wt%) may block the pores of support and also thus decrease the gravimetric capacity and ECA of the material studied [92].

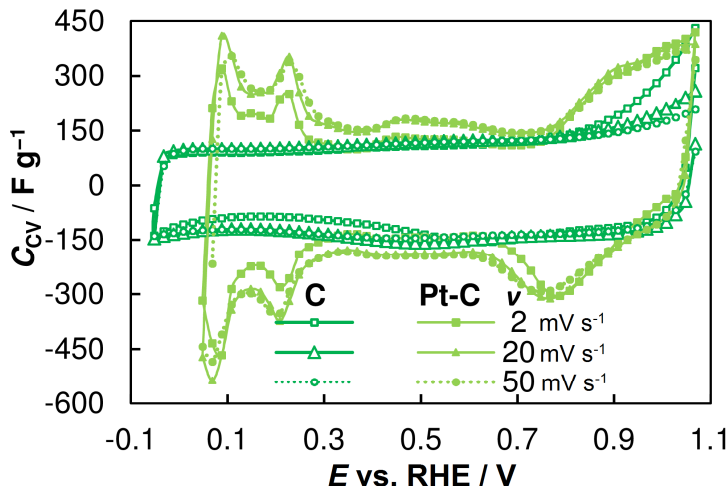


Figure 12. Gravimetric capacitance, C_{CV} , vs. electrode potential, E , curves for C(Mo₂C)800 °C (empty markers) and Pt-C(Mo₂C)800 °C electrodes (filled markers) in 0.5 M H₂SO₄ solution saturated with Ar at different potential scan rates v , given in the figure.

The values of gravimetric capacitance, C_{CV} , were calculated from the CV curves for C(Mo₂C)800 °C and Pt-C(Mo₂C)800 °C electrodes (Fig. 12). As the specific surface area for CDC support is very high, the behaviour of the system is highly capacitive. Analysis of CV data shows that the high gravimetric capacitance (calculated from CV data) values (150 F g⁻¹) have been established for both CDC and Pt-CDC electrodes. Cycling the potential from negative potential values towards positive potentials, the carbon support starts to oxidize at E more positive than 0.90 V vs. RHE. For Pt nanocluster-activated CDC, distinct regions of cathodic hydrogen evolution and adsorption–desorption of hydrogen at $E < 0.30$ vs. RHE are clearly visible. The region of Pt surface oxide formation is present in the anodic scan at $E > 0.80$ V vs. RHE. The surface oxide is reduced at the cathodic scan with peak current at $E = 0.78$ V vs. RHE [17].

It was concluded, that C(Mo₂C)800 °C is promising material for PEMFC electrode support having more suitable properties than C(WC)1100 °C, C(Mo₂C)1000 °C and commercial carbon Vulcan XC72R. CDCs with high gravimetric capacitance [17] and electrochemical activity could be used as the electrode materials for combined energy storage/regenerating devices.

6.3 Electrochemical characterization of Pt-C(Mo₂C) electrodes in PEM single cells

Based on the three-electrode experiments on GCDE [17,21,86,92], it was decided to test Pt-C(Mo₂C) in the single cell. The C(Mo₂C) materials synthesized from 600 °C to 1000 °C are interesting objects as their physical properties like graphitization level and pore size distribution vary to a great extent [21] and therefore comparing these materials with commercial carbon Vulcan XC72R could give valuable information about the influence of the properties of catalyst support materials on the performance of PEMFC. Moreover, previous experiments showed [21], that the carbon materials studied like C(Mo₂C)750 °C, C(Mo₂C)800 °C and C(Mo₂C)850 °C could be the most suitable for PEMFC application. The single cell tests were conducted with:

- (a) symmetrical (Pt-CDC | Nafion[®] | Pt-CDC) and
- (b) asymmetrical (Pt-CDC | Nafion[®] | Pt-C(Vulcan)) arrangement to test the novel materials at both electrodes of the single cell.

6.3.1 The polarization and power density curves

In Fig. 13 the polarization (j , ΔE) and power density (j , P) curves for PEMFC single cells with different electrodes are presented. The data for symmetrical (a) and asymmetrical (b) single cells using different C(Mo₂C) and C(Vulcan) as catalyst support are shown. In asymmetrical single cells MEAs were prepared using Pt-nanoclusters activated Pt-C(Mo₂C) as cathodes and Pt-C(Vulcan) as anodes. At constant cell potential ($\Delta E = 0.6$ V) for symmetrical single cells the

current density increases in the order: Pt-C(Mo₂C)1000 °C < Pt-C(Mo₂C)900 °C < Pt-C(Vulcan) < Pt-C(Mo₂C)800 °C ≈ Pt-C(Mo₂C)750 °C < Pt-C(Mo₂C)600 °C < Pt-C(Mo₂C)850 °C. For asymmetrical single cells the corresponding data are fairly similar with the current density increasing in the order of cathode materials: Pt-C(Mo₂C)1000 °C < Pt-C(Mo₂C)900 °C < Pt-C(Vulcan) < Pt-C(Mo₂C)600 °C < Pt-C(Mo₂C)850 °C < Pt-C(Mo₂C)800 °C ≈ Pt-C(Mo₂C)750 °C. The maximum power density of the single cells studied increases in the same order. It should be noted that comparable order of catalysts has been established for ORR activity in aqueous 0.5 M H₂SO₄ solution in the three-electrode system measured using different CDCs synthesized from Mo₂C [21]. Based on these data it can be concluded that the activity of symmetrical and asymmetrical single cell is controlled by the electroreduction activity of O₂ at the cathode and the influence of the anode composition for H₂ oxidation rate is very small.

The variation in the current and power densities for the materials studied can be explained mainly with the increase of the total pore volume of the cathode materials used in single cells (data given in Table 2). The symmetrical single cells based on C(Mo₂C) carbon powders, that were synthesised at temperature within the range from 600 to 850 °C demonstrated higher power values than the Vulcan based symmetrical single cell, which to the first approximation could be explained by the higher total pore volume of C(Mo₂C) based electrodes. For asymmetrical single cells the highest power values were demonstrated by MEAs with Pt-C(Mo₂C)800 °C and Pt-C(Mo₂C)750 °C cathodes. However much lower power values were reached by single cells with cathode materials Pt-C(Mo₂C)1000 °C and Pt-C(Mo₂C)900 °C which have moderate total pore volume. This could be explained by relatively low specific surface area and mesopore volume values. The symmetrical single cell completed from Pt-C(Vulcan) has intermediate activity. Uchida et al. [12] found that the acetylene blacks are suitable catalyst supports for PEMFCs. The high electrochemical activity has been explained by the large amount of meso- and macropores (i.e. secondary pores) within the electrode material (i.e. pores from 0.05 to 1.0 μm [12]). Probably the secondary pores in the mesoporous-macroporous carbon support help to achieve good contact between gas phase (quick O₂ transport to catalytically active areas), electrolyte, catalyst support and Pt nanoparticles.

Starting from the cell potential corresponding to maximum power density, the processes in the working single cell are mainly limited by the diffusion (mass transfer) step rate [93]. In this region, at $\Delta E = 0.6 \dots 0.9$ V, the current density values for Pt-C(Mo₂C) based fuel cells are noticeably higher than that for the Pt-C(Vulcan) based symmetrical system. These differences in the activity of the PEMFC single cells are probably caused by the enhanced rate of reactants and products mass-transfer (and ORR) rate at the Pt-C(Mo₂C)600 °C, Pt-C(Mo₂C)750 °C, Pt-C(Mo₂C)800 °C and Pt-C(Mo₂C)850 °C cathodes. Effective O₂ mass transfer and water management among of the Pt-nanoclusters activated carbon materials is extremely important when high currents are applied to a FC.

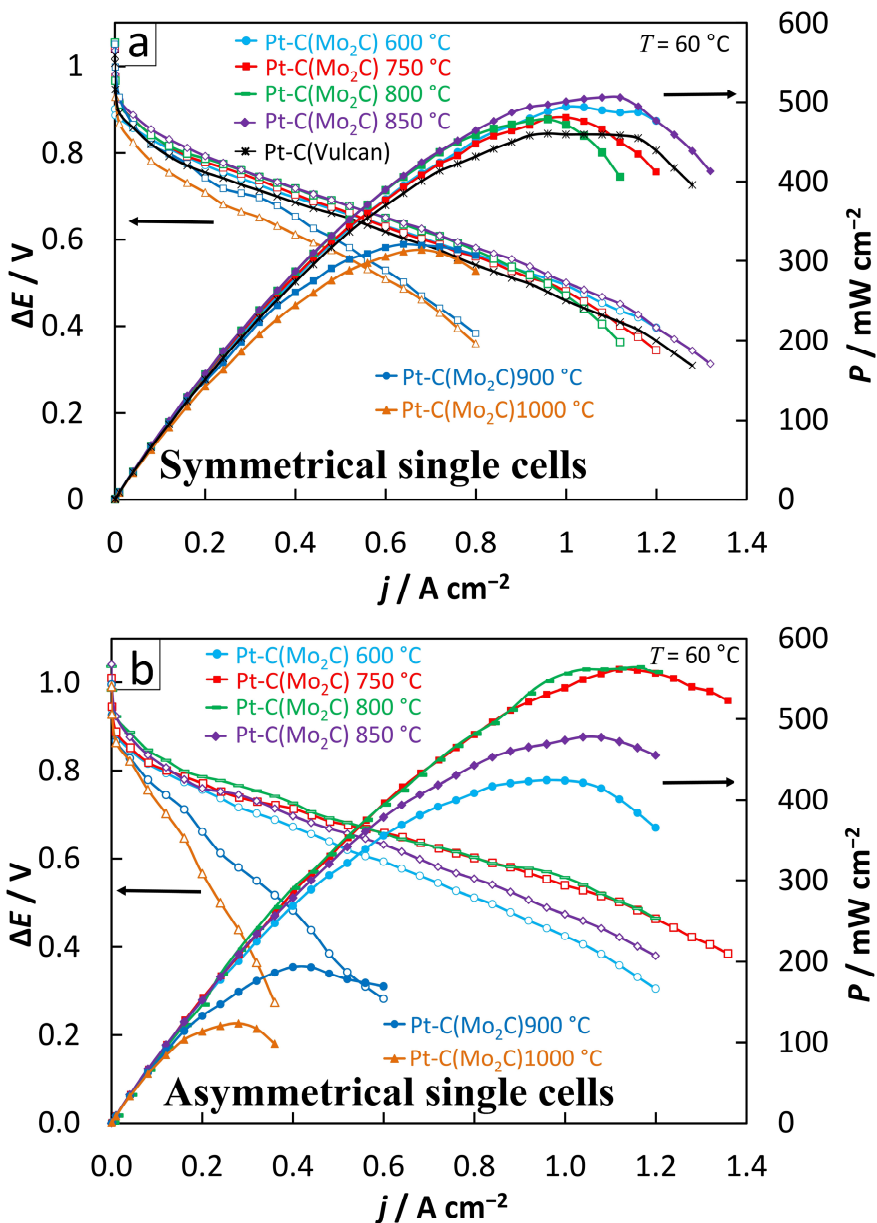


Figure 13. The polarization (j , ΔE) and power density vs. current density (j , ΔP) curves for a) symmetrical and b) asymmetrical single cells with different electrode materials (noted in figure). In asymmetrical single cell Pt-C(Vulcan) is used as anode for all MEAs. Measurements conditions: $T = 60\text{ }^{\circ}\text{C}$, atmospheric pressure and gases with 100% relative humidity gases were fed to electrodes at flow rate of $200\text{ cm}^3\text{ min}^{-1}$.

6.3.2 CV and EIS data for single cells studied

To obtain further explanations of the reasons behind the very good activity and stability of the Pt-C(Mo₂C) based single cells, nitrogen was fed to the cathode and the ECA values have been estimated at fixed temperature ($T = 30\text{ }^{\circ}\text{C}$). As seen in Fig. 14, there are very nice and clear current peaks in the CVs within the region of the formation (adsorption) and oxidation (desorption) of hydrogen adatoms (from 0 to 0.4 V vs. RHE). The very high C_{CV} values indicate, that these single cells can be used as peak energy (supercapacitor like) generating devices [19–22,42–45].

For all single cells studied ECA was calculated using equations 12 and 13. The material Pt-C(Mo₂C)800 °C demonstrated the highest ECA value (11.9 m² g⁻¹), which is comparable with ECA values determined in the three-electrode experiments [21]. For other Pt-C(Mo₂C) materials the ECA values are slightly lower, except for the Pt-C(Mo₂C)900 °C and Pt-C(Mo₂C)1000 °C catalysts, demonstrating very low ECA values. As the crystallite sizes of platinum for all materials prepared are relatively similar (Table 2), the differences in the values of ECA and total activity of PEM single cells have been probably caused by the mass transport rate differences of H₃O⁺ and O₂ into the porous catalysts or by contact resistance of Nafion[®] with Pt nanoparticles at the three boundary interface.

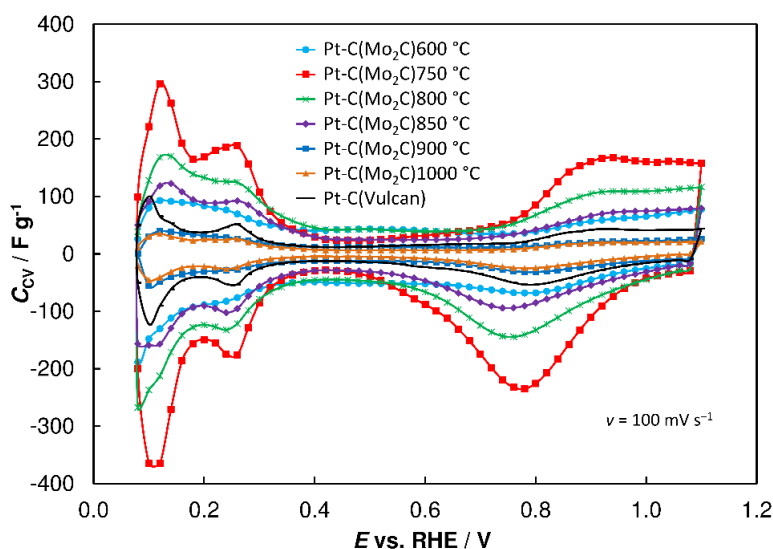


Figure 14. The cyclic voltammograms for single cells with different cathodes studied. Measurement conditions are as follows: cell temperature 30 °C, hydrogen flow rate 10 cm³ min⁻¹ at the anode side, nitrogen flow rate 200 cm³ min⁻¹ at the cathode side (both gases with 100% relative humidity), scan rate is 100 mV s⁻¹.

Fig. 15 presents the Nyquist plots for a) symmetrical and b) asymmetrical single cells studied ($\Delta E = 0.55$ V). It can be seen that plots for symmetrical and asymmetrical single cells follow the same trend and the pore size distribution of the (cathode) catalyst materials has great influence on the total polarization resistance values of the single cell. Thus, the microporosity-mesoporosity has a noticeable effect on the kinetics of ORR. The catalyst materials with higher mesopore volume (e.g. Pt-C(Mo₂C)800 °C and Pt-C(Mo₂C)850 °C) have much lower polarization resistances than the materials with lower mesopore volume (e.g. Pt-C(Mo₂C)900 °C and Pt-C(Mo₂C)1000 °C). Very high polarization resistance values for Pt-C(Mo₂C)1000 °C based PEMFC single cell can be explained also by the partial graphitisation of the carbon substrate layers (decreasing the number of catalytic centres) as well as by decreasing the mass transport rate of oxygen into less porous structure of the catalysts [16,94].

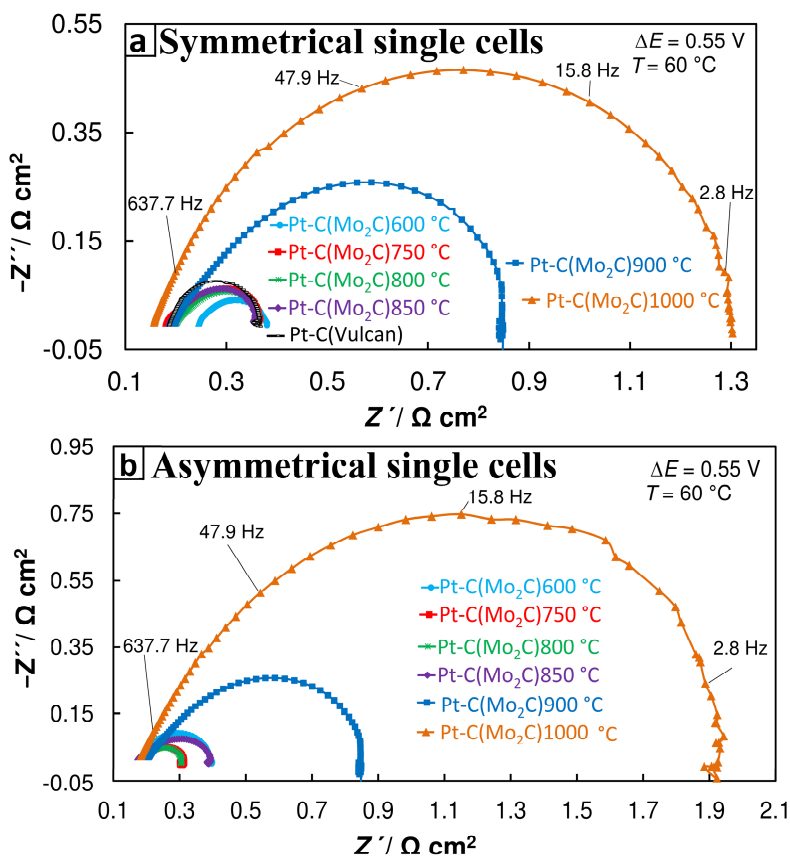


Figure 15. Nyquist plots for: a) symmetrical and b) asymmetrical single cells with different electrode materials (noted in figure). For asymmetrical single cell Pt-C(Vulcan) is an anode for all MEAs. Measurements conditions were following: cell potential $\Delta E = 0.55$ V $T = 60$ °C, atmospheric pressure and with 100% relative humidity, O₂ and H₂ were fed to electrodes at flow rate of 200 cm³ min⁻¹.

6.3.3 Time stability tests

Electrochemical time stability is very important for FC catalysts and therefore the MEAs were tested in constant current regime ($j = 0.4 \text{ A cm}^{-2}$) at $60 \text{ }^\circ\text{C}$ for 160 h (Fig. 16). Under these conditions the symmetrical MEA prepared from Pt-C(Mo₂C)750 °C exhibited much lower potential drop rate ($\Delta E/\Delta t = 240 \text{ } \mu\text{V h}^{-1}$) than the MEA prepared from Pt-C(Vulcan) ($\Delta E/\Delta t = 670 \text{ } \mu\text{V h}^{-1}$) (Fig. 16). The Pt-C(Mo₂C)750 °C symmetrical single cell was tested further, applying same conditions so that the total time at constant current reached 600 h. The potential drop rate between 160 h and 600 h was $165 \text{ } \mu\text{V h}^{-1}$ being slightly lower than the initial value.

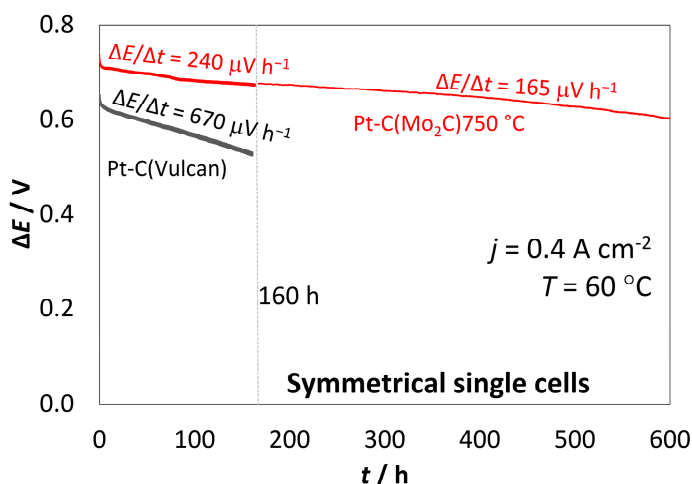


Figure 16. Lifetime measurements of the symmetrical Pt-C(Mo₂C)750 °C and Pt-C(Vulcan) single cells (noted in figure) at constant current polarization regime ($j = 0.4 \text{ A cm}^{-2}$) at $60 \text{ }^\circ\text{C}$. Measurements conditions: atmospheric pressure, gases with 100% relative humidity gases were fed to electrodes at flow rate $50 \text{ cm}^3 \text{ min}^{-1}$.

The polarization and power density curves were measured before and after 160 h lifetime tests and are given in Fig 17. In the course of this test the maximum power density value for single cell with Pt-C(Mo₂C)750 °C electrodes decreased 5% from 460 mW cm^{-2} to 440 mW cm^{-2} . However, for Pt-C(Vulcan) based single cell the damage was much more severe with maximum power density value decreasing from 460 mW cm^{-2} to 320 mW cm^{-2} (i.e. 30% power drop). The damage was probably mainly caused by carbon corrosion, growth of platinum particles, dissolution and detachment of platinum particles from the carbon support. It must be noted that the OCP values did not change within durability tests, indicating that the decrease of single cell performance is caused by degradation of the electrodes and not by increasing H₂ leak through Nafion[®] membrane.

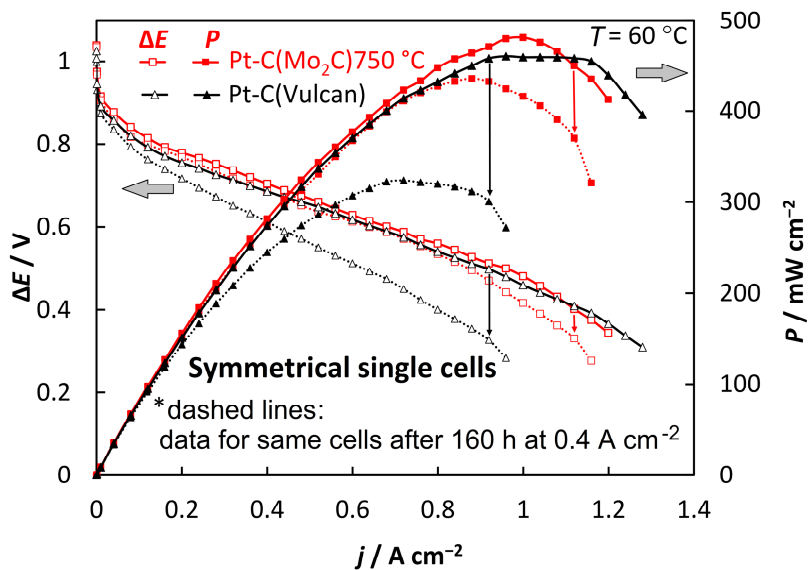


Figure 17. The polarization and power density curves for the symmetrical Pt-C(Mo_2C)750 $^\circ\text{C}$ and Pt-C(Vulcan) single cells before and after the lifetime tests (noted in figure). Measurements conditions: $T = 60 \text{ }^\circ\text{C}$, atmospheric pressure, gases with 100% relative humidity gases were fed to electrodes at flow rate $200 \text{ cm}^3 \text{ min}^{-1}$.

7. SUMMARY

Carbide-derived carbons (CDCs) have been synthesized from Mo_2C and WC powders by high-temperature chlorination from 600 °C to 1100 °C to test suitability of catalyst supports in polymer electrolyte membrane fuel cell (PEMFC) application. Prepared carbon materials were compared with commercial carbon Vulcan XC72R (C(Vulcan)) using different characterization methods. Activated Pt-CDCs and Pt-C(Vulcan) have been prepared using so-called sodium borohydride reduction method. Carbon supports and Pt-activated catalyst materials were tested in the H_2SO_4 aqueous solution in the three-electrode configuration and thereafter catalyst materials were used in the single cell measurements.

Experiments in the three-electrode cell indicate that graphitization level and pore size distribution have great impact on oxygen electroreduction reaction (ORR). The synthesized CDCs are more active for the ORR and demonstrate higher kinetic current density values than C(Vulcan). Due to the more optimal structure of the carbon supports (the number of defects and the ratio of micro- and mesopores), the electrochemical activity of C(Mo_2C)800 °C is higher than that of C(WC)1100 °C and especially that of C(Vulcan).

Fuel cell membrane electrode assemblies were prepared and tested in polymer electrolyte membrane fuel cell (PEMFC) single cells using catalyst supports prepared from Mo_2C derived carbons and commercial Vulcan XC72. It was established that CDCs prepared from Mo_2C at different chlorination temperatures from 600 to 1000 °C can be used in the PEMFC application. Physical properties of the carbon supports like crystal structure, specific surface area and pore size distribution (micropore and mesopore volume) have great influence on the PEMFC parameters, especially on the maximum power density value. It was shown, that the mesopore volume of the cathode support material is a very important parameter due to the limitations of mass transport of O_2 in the fuel cell working conditions. The most suitable synthesis temperature range for C(Mo_2C) is from 750 to 850 °C as Pt-C(Mo_2C)750 °C, Pt-C(Mo_2C)800 °C and Pt-C(Mo_2C)850 °C catalysts have suitable pore size distribution, microporosity-mesoporosity ratios, and MEAs prepared using these materials exhibited the highest power density values. Comparison of symmetrical and asymmetrical MEAs demonstrated that the role of anode composition is not very important and the efficiency of a fuel cell is determined by ORR at the cathode when pure H_2 is used as a fuel.

The results established for the Pt-C(Mo_2C) based electrodes were compared with those for commercial Vulcan XC72 based MEAs and more than 10% increase in power density was achieved due to the higher specific surface area and more suitable pore size distribution. Time stability test showed lower degradation for Pt-C(Mo_2C)750 °C than Pt-C(Vulcan) based PEM single cell: cell potential loss rates during 160 h at 0.4 A cm^{-2} and 60 °C were 240 $\mu\text{V h}^{-1}$ and 670 $\mu\text{V h}^{-1}$ respectively. Based on the information collected, it can be concluded that CDCs are promising catalysts support materials and Pt-nanoclusters activated CDCs can be used as the catalysts for PEMFC demonstrating suitable physical properties and therefore high efficiency and good durability.

8. REFERENCES

- [1] S. Shahgaldi, J. Hamelin, Improved carbon nanostructures as a novel catalyst support in the cathode side of PEMFC: a critical review, *Carbon*. 94 (2015) 705–728.
- [2] D. Rohendi, E.H. Majlan, A.B. Mohamad, W.R. Wan Daud, A.A. Hassan Kadhum, L.K. Shyuan, Characterization of electrodes and performance tests on MEAs with varying platinum content and under various operational conditions, *Int. J. Hydrog. Energy*. 38 (2013) 9431–9437.
- [3] Y.-C. Park, K. Kakinuma, M. Uchida, H. Uchida, M. Watanabe, Deleterious effects of interim cyclic voltammetry on Pt/carbon black catalyst degradation during start-up/shutdown cycling evaluation, *Electrochim. Acta*. 123 (2014) 84–92.
- [4] M.K. Debe, Electrocatalyst approaches and challenges for automotive fuel cells, *Nature*. 486 (2012) 43–51.
- [5] O.A. Petrii, Pt–Ru electrocatalysts for fuel cells: a representative review, *J. Solid State Electrochem.* 12 (2008) 609–642.
- [6] T.J. Schmidt, Characterization of high-surface-area electrocatalysts using a rotating disk electrode configuration, *J. Electrochem. Soc.* 145 (1998) 2354.
- [7] Z.-B. Wang, C.-R. Zhao, P.-F. Shi, Y.-S. Yang, Z.-B. Yu, W.-K. Wang, G.-P. Yin, Effect of a carbon support containing large mesopores on the performance of a Pt–Ru–Ni/C catalyst for direct methanol fuel cells, *J. Phys. Chem. C*. 114 (2010) 672–677.
- [8] K. Sasaki, Y. Mo, J.X. Wang, M. Balasubramanian, F. Uribe, J. McBreen, R.R. Adzic, Pt submonolayers on metal nanoparticles—novel electrocatalysts for H₂ oxidation and O₂ reduction, *Electrochim. Acta*. 48 (2003) 3841–3849.
- [9] C.J. Corcoran, H. Tavassol, M.A. Rigsby, P.S. Bagus, A. Wieckowski, Application of XPS to study electrocatalysts for fuel cells, *J. Power Sources*. 195 (2010) 7856–7879. doi:10.1016/j.jpowsour.2010.06.018.
- [10] L. Du, Y. Shao, J. Sun, G. Yin, J. Liu, Y. Wang, Advanced catalyst supports for PEM fuel cell cathodes, *Nano Energy*. (n.d.). doi:10.1016/j.nanoen.2016.03.016.
- [11] M. Uchida, Y.-C. Park, K. Kakinuma, H. Yano, D.A. Tryk, T. Kamino, H. Uchida, M. Watanabe, Effect of the state of distribution of supported Pt nanoparticles on effective Pt utilization in polymer electrolyte fuel cells, *Phys. Chem. Chem. Phys.* 15 (2013) 11236–11247.
- [12] M. Uchida, Y. Fukuoka, Y. Sugawara, N. Eda, A. Ohta, Effects of Microstructure of Carbon Support in the Catalyst Layer on the Performance of Polymer-Electrolyte Fuel Cells, *J. Electrochem. Soc.* 143 (1996) 2245–2252.
- [13] S. Gottesfeld, I.D. Raistrick, S. Srinivasan, Oxygen reduction kinetics on a platinum RDE coated with a recast Nafion film, *J. Electrochem. Soc.* 134 (1987) 1455–1462.
- [14] G.S. Chai, S.B. Yoon, J.-S. Yu, J.-H. Choi, Y.-E. Sung, Ordered porous carbons with tunable pore sizes as catalyst supports in direct methanol fuel cell, *J Phys Chem B*. 108 (2004) 7074–7079.
- [15] E. Antolini, Carbon supports for low-temperature fuel cell catalysts, *Appl. Catal. B Environ.* 88 (2009) 1–24.
- [16] S. Sepp, K. Vaarmets, J. Nerut, I. Tallo, E. Tee, H. Kurig, J. Aruväli, R. Kanarbik, E. Lust, Performance of Polymer Electrolyte Membrane Fuel Cell Single Cells Prepared Using Hierarchical Microporous-Mesoporous Carbon

- Supported Pt Nanoparticles Activated Catalysts, *Electrochim. Acta.* 203 (2016) 221–229.
- [17] S. Sepp, E. Härk, P. Valk, K. Vaarmets, J. Nerut, R. Jäger, E. Lust, Impact of the Pt catalyst on the oxygen electroreduction reaction kinetics on various carbon supports, *J. Solid State Electrochem.* 18 (2014) 1223–1229.
- [18] A. Jänes, H. Kurig, E. Lust, Characterisation of activated nanoporous carbon for supercapacitor electrode materials, *Carbon.* 45 (2007) 1226–1233.
- [19] Y. Gogotsi, A. Nikitin, H. Ye, W. Zhou, J.E. Fischer, B. Yi, H.C. Foley, M.W. Barsoum, Nanoporous carbide-derived carbon with tunable pore size, *Nat. Mater.* 2 (2003) 591–594.
- [20] E. Lust, E. Härk, J. Nerut, K. Vaarmets, Pt and Pt–Ru catalysts for polymer electrolyte fuel cells deposited onto carbide-derived carbon supports, *Electrochim. Acta.* 101 (2013) 130–141.
- [21] E. Lust, K. Vaarmets, J. Nerut, I. Tallo, P. Valk, S. Sepp, E. Härk, Influence of specific surface area and microporosity-mesoporosity of pristine and Pt-nanoclusters modified carbide derived carbon electrodes on the oxygen electroreduction, *Electrochim. Acta.* 140 (2014) 294–303.
- [22] L. Borchardt, F. Hasché, M.R. Lohe, M. Oschatz, F. Schmidt, E. Kockrick, C. Ziegler, T. Lescouet, A. Bachmatiuk, B. Büchner, D. Farrusseng, P. Strasser, S. Kaskel, Transition metal loaded silicon carbide-derived carbons with enhanced catalytic properties, *Carbon.* 50 (2012) 1861–1870.
- [23] E. Härk, J. Nerut, K. Vaarmets, I. Tallo, H. Kurig, J. Eskusson, K. Kontturi, E. Lust, Electrochemical impedance characteristics and electroreduction of oxygen at tungsten carbide derived micromesoporous carbon electrodes, *J. Electroanal. Chem.* 689 (2013) 176–184.
- [24] K. Vaarmets, S. Sepp, J. Nerut, E. Härk, I. Tallo, E. Lust, Electrochemical and physical characterization of Pt–Ru alloy catalyst deposited onto microporous–mesoporous carbon support derived from Mo₂C at 600 °C, *J. Solid State Electrochem.* 17 (2013) 1729–1741.
- [25] R. Schlögl, *Chemical Energy Storage*, Walter de Gruyter, 2013.
- [26] A.A. Franco, *Polymer Electrolyte Fuel Cells: Science, Applications, and Challenges*, CRC Press, 2016.
- [27] F. Barbir, *PEM Fuel Cells. Theory and Practice*, Elsevier Inc., United States of America, 2013.
- [28] U.S Department of Energy, Office of Energy Efficiency and Renewable Energy, U.S. DRIVE Fuel Cell Tech Team Cell Component Accelerated Stress Test and Polarization Curve Protocols for PEM Fuel Cells, (2013).
- [29] U.S Department of Energy, Office of Fossil Energy, National Energy Technology Laboratory, *Fuel Cell Handbook*, 7th ed., EG&G Technical Services, Inc., Morgantown, West Virginia, 2004.
- [30] Y. Shao-Horn, W.C. Sheng, S. Chen, P.J. Ferreira, E.F. Holby, D. Morgan, Instability of supported platinum nanoparticles in low-temperature fuel cells, *Top. Catal.* 46 (2007) 285–305.
- [31] P. Trogadas, T.F. Fuller, P. Strasser, Carbon as catalyst and support for electrochemical energy conversion, *Carbon.* 75 (2014) 5–42.
- [32] B.C.H. Steele, A. Heinzel, Materials for fuel-cell technologies, *Nature.* 414 (2001) 345–352.
- [33] E. Antolini, Formation of carbon-supported PtM alloys for low temperature fuel cells: a review, *Mater. Chem. Phys.* 78 (2003) 563–573.

- [34] B. Wang, Recent development of non-platinum catalysts for oxygen reduction reaction, *J. Power Sources*. 152 (2005) 1–15.
- [35] P. Zihrul, I. Hartung, S. Kirsch, G. Huebner, F. Hasché, H.A. Gasteiger, Voltage Cycling Induced Losses in Electrochemically Active Surface Area and in H₂/Air-Performance of PEM Fuel Cells, *J. Electrochem. Soc.* 163 (2016) F492–F498.
- [36] E. Antolini, Structural parameters of supported fuel cell catalysts: The effect of particle size, inter-particle distance and metal loading on catalytic activity and fuel cell performance, *Appl. Catal. B Environ.* 181 (2016) 298–313.
- [37] P. Gallezot, S. Chaumet, A. Perrard, P. Isnard, Catalytic Wet Air Oxidation of Acetic Acid on Carbon-Supported Ruthenium Catalysts, *J. Catal.* 168 (1997) 104–109.
- [38] B. Wickman, H. Grönbeck, P. Hanarp, B. Kasemo, Corrosion Induced Degradation of Pt/C Model Electrodes Measured with Electrochemical Quartz Crystal Microbalance, *J. Electrochem. Soc.* 157 (2010) B592–B598.
- [39] L.M. Roen, C.H. Paik, T.D. Jarvi, Electrocatalytic Corrosion of Carbon Support in PEMFC Cathodes, *Electrochem. Solid-State Lett.* 7 (2004) A19–A22.
- [40] G. Álvarez, F. Alcaide, O. Miguel, L. Calvillo, M. Lázaro, J. Quintana, J. Calderón, E. Pastor, Technical electrodes catalyzed with PtRu on mesoporous ordered carbons for liquid direct methanol fuel cells, *J. Solid State Electrochem.* 14 (2010) 1027–1034.
- [41] A. Jänes, T. Thomberg, E. Lust, Synthesis and characterisation of nanoporous carbide-derived carbon by chlorination of vanadium carbide, *Carbon*. 45 (2007) 2717–2722.
- [42] I. Tallo, T. Thomberg, A. Jänes, E. Lust, Electrochemical behavior of α -tungsten carbide-derived carbon based electric double-layer capacitors, *J. Electrochem. Soc.* 159 (2012) A208–A213.
- [43] I. Tallo, T. Thomberg, K. Kontturi, A. Jänes, E. Lust, Nanostructured carbide-derived carbon synthesized by chlorination of tungsten carbide, *Carbon*. 49 (2011) 4427–4433.
- [44] A. Jänes, T. Thomberg, H. Kurig, E. Lust, Nanoscale fine-tuning of porosity of carbide-derived carbon prepared from molybdenum carbide, *Carbon*. 47 (2009) 23–29.
- [45] T. Thomberg, A. Jänes, E. Lust, Energy and power performance of vanadium carbide derived carbon electrode materials for supercapacitors, *J. Electroanal. Chem.* 630 (2009) 55–62.
- [46] Y. Gogotsi, ed., Carbide-Derived Carbon, in: *Nanomater. Handb.*, CRC Press, Boca Raton, 2006: pp. 250–293.
- [47] E. Tee, I. Tallo, H. Kurig, T. Thomberg, A. Jänes, E. Lust, Huge enhancement of energy storage capacity and power density of supercapacitors based on the carbon dioxide activated microporous SiC-CDC, *Electrochim. Acta.* 161 (2015) 364–370.
- [48] K. Kinoshita, *Electrochemical oxygen technology*, John Wiley and Sons, INC., New York, 1992.
- [49] R. Adžić, J. Lipkowski, P.N. Ross, *Electrocatalysis*, Wiley-VCH, New York, 1998.
- [50] K. Kinoshita, *Electrochemical oxygen technology*, John Wiley and Sons, INC., New York, 1992.

- [51] N.M. Marković, R.R. Adžić, B.D. Cahan, E.B. Yeager, Structural effects in electrocatalysis: oxygen reduction on platinum low index single-crystal surfaces in perchloric acid solutions, *J. Electroanal. Chem.* 377 (1994) 249–259.
- [52] J. Rossmeisl, G.S. Karlberg, T. Jaramillo, J.K. Nørskov, Steady state oxygen-reduction and cyclic voltammetry, *Faraday Discuss.* 140 (2009) 337–346.
- [53] M. Gara, R.G. Compton, Activity of carbon electrodes towards oxygen reduction in acid: A comparative study, *New J. Chem.* 35 (2011) 2647–2652.
- [54] A. Schlange, A.R. dos Santos, B. Hasse, B.J.M. Etzold, U. Kunz, T. Turek, Titanium carbide-derived carbon as a novel support for platinum catalysts in direct methanol fuel cell application, *J. Power Sources.* 199 (2012) 22–28.
- [55] P. Giannozzi, S. Baroni, N. Bonini, M. Calandra, R. Car, C. Cavazzoni, D. Ceresoli, G.L. Chiarotti, M. Cococcioni, I. Dabo, A.D. Corso, S. de Gironcoli, S. Fabris, G. Fratesi, R. Gebauer, U. Gerstmann, C. Gougoussis, A. Kokalj, M. Lazzeri, L. Martin-Samos, N. Marzari, F. Mauri, R. Mazzarello, S. Paolini, A. Pasquarello, L. Paulatto, C. Sbraccia, S. Scandolo, G. Sclauzero, A.P. Seitsonen, A. Smogunov, P. Umari, R.M. Wentzcovitch, QUANTUM ESPRESSO: a modular and open-source software project for quantum simulations of materials, *J. Phys. Condens. Matter.* 21 (2009) 395502.
- [56] M. Thommes, Physical Adsorption Characterization of Nanoporous Materials, *Chem. Ing. Tech.* 82 (2010) 1059–1073.
- [57] E. Fitzer, K.-H. Kochling, H.P. Boehm, H. Marsh, Recommended terminology for the description of carbon as a solid (IUPAC Recommendations 1995), *Pure Appl. Chem.* 67 (1995).
- [58] S. Brunauer, P.H. Emmett, E. Teller, Adsorption of Gases in Multimolecular Layers, *J. Am. Chem. Soc.* 60 (1938) 309–319. doi:10.1021/ja01269a023.
- [59] S. Lowell, J.E. Shields, M.A. Thomas, M. Thommes, Adsorption Isotherms, in: *Charact. Porous Solids Powders Surf. Area Pore Size Density*, Springer Netherlands, 2004: pp. 11–14.
- [60] F. Rouquerol, J. Rouquerol, K. Sing, Chapter 6 – Assessment of Surface Area, in: *F. Rouquerol, J. Rouquerol, K. Sing (Eds.), Adsorpt. Powders Porous Solids*, Academic Press, London, 1999: pp. 165–189.
- [61] D.D. Do, *Adsorption Analysis: Equilibria and Kinetics*, Imperial College Press, London, 1998.
- [62] S.J. Gregg, K.S.W. Sing, *Adsorption, surface area, and porosity*, Academic Press, 1991.
- [63] S. Lowell, J.E. Shields, M.A. Thomas, M. Thommes, Chemisorption: Site Specific Gas Adsorption, in: *Charact. Porous Solids Powders Surf. Area Pore Size Density*, Springer Netherlands, 2004: pp. 213–233.
- [64] J.H. de Boer, B.C. Lippens, B.G. Linsen, J.C.P. Broekhoff, A. van den Heuvel, T.J. Osinga, The t-curve of multimolecular N₂-adsorption, *J. Colloid Interface Sci.* 21 (1966) 405–414.
- [65] R. Evans, U.M.B. Marconi, P. Tarazona, Fluids in narrow pores: Adsorption, capillary condensation, and critical points, *J. Chem. Phys.* 84 (1986) 2376–2399.
- [66] P.I. Ravikovitch, A.V. Neimark, Characterization of nanoporous materials from adsorption and desorption isotherms, *Colloids Surf. Physicochem. Eng. Asp.* 187–188 (2001) 11–21. doi:10.1016/S0927-7757(01)00614-8.
- [67] P.E.J. Flewitt, R.K. Wild, *Physical Methods for Materials Characterisation*, 2th ed., Taylor & Francis, 2003.

- [68] D.A. Skoog, F.J. Holler, T.A. Nieman, Principles of instrumental analysis, Saunders College Pub., Philadelphia; London, 1998.
- [69] A.L. Patterson, The Scherrer Formula for X-Ray Particle Size Determination, *Phys. Rev.* 56 (1939) 978–982.
- [70] A.J. Bard, L.R. Faulkner, *Electrochemical methods: fundamentals and applications*, Wiley, New York, 2001.
- [71] S. Trasatti, O.A. Petrii, An International Journal Devoted to all Aspects of Electrode Kinetics, Interfacial Structure, Properties of Electrolytes, Colloid and Biological Electrochemistry Real surface area measurements in electrochemistry, *J. Electroanal. Chem.* 327 (1992) 353–376.
- [72] F.J. Nores-Pondal, I.M.J. Vilella, H. Troiani, M. Granada, S.R. de Miguel, O.A. Scelza, H.R. Corti, Catalytic activity vs. size correlation in platinum catalysts of PEM fuel cells prepared on carbon black by different methods, *Int. J. Hydrog. Energy.* 34 (2009) 8193–8203.
- [73] S. Gottesfeld, I.D. Raistrick, S. Srinivasan, Oxygen reduction kinetics on a platinum RDE coated with a recast Nafion film, *J. Electrochem. Soc.* 134 (1987) 1455–1462.
- [74] V.S. Bagotsky, *Fundamentals of Electrochemistry*, John Wiley & Sons, 2005.
- [75] C.M.A. Brett, A.M.O. Brett, *Electrochemistry: Principles, Methods, and Applications*, Oxford University Press, Incorporated, 1993.
- [76] E. Gileadi, *Electrode Kinetics for Chemists, Chemical Engineers and Materials Scientists*, Wiley, 1993.
- [77] T.J.S. U. A. Paulus, Oxygen reduction on a high-surface area Pt/Vulcan carbon catalyst: a thin-film rotating ring-disk electrode study, *J. Electroanal. Chem.* (2001) 134–145.
- [78] S.S. Kocha, Y. Garsany, D. Myers, *Testing Oxygen Reduction Reaction Activity with the Rotating Disc Electrode Technique*, (2013).
- [79] T.J. Schmidt, H.A. Gasteiger, G.D. Stäb, P.M. Urban, D.M. Kolb, R.J. Behm, Characterization of High-Surface-Area Electrocatalysts Using a Rotating Disk Electrode Configuration, *J. Electrochem. Soc.* 145 (1998) 2354–2358.
- [80] G.A. Ragoisha, A.S. Bondarenko, Potentiodynamic electrochemical impedance spectroscopy, *Electrochim. Acta.* 50 (2005) 1553–1563.
- [81] R. Borup, J. Meyers, B. Pivovar, Y.S. Kim, R. Mukundan, N. Garland, D. Myers, M. Wilson, F. Garzon, D. Wood, P. Zelenay, K. More, K. Stroh, T. Zawodzinski, J. Boncella, J.E. McGrath, M. Inaba, K. Miyatake, M. Hori, K. Ota, Z. Ogumi, S. Miyata, A. Nishikata, Z. Siroma, Y. Uchimoto, K. Yasuda, K. Kimijima, N. Iwashita, Scientific Aspects of Polymer Electrolyte Fuel Cell Durability and Degradation, *Chem. Rev.* 107 (2007) 3904–3951.
- [82] P.J. Ferreira, G.J. la O^o, Y. Shao-Horn, D. Morgan, R. Makharia, S. Kocha, H.A. Gasteiger, Instability of Pt/C Electrocatalysts in Proton Exchange Membrane Fuel Cells A Mechanistic Investigation, *J. Electrochem. Soc.* 152 (2005) A2256–A2271.
- [83] V. Lakshminarayanan, R. Srinivasan, D. Chu, S. Gilman, Area determination in fractal surfaces of Pt and PtRu electrodes, *Surf. Sci.* 392 (1997) 44–51.
- [84] H. Kurig, M. Russina, I. Tallo, M. Siebenbürger, T. Romann, E. Lust, Thactae suitability of infinite slit-shaped pore model to describe the pores in highly porous carbon materials, *Carbon.* 100 (2016) 617–624.
- [85] E. Härk, V. Steinberg, S. Sepp, K. Vaarmets, J. Nerut, T. Kallio, K. Kontturi, E. Lust, *Electrochemical and Physical Characterization of Pt Activated*

- Micromesoporous Vanadium Carbide Derived Carbon Electrodes in Sulfuric Acid Solution, *J. Electrochem. Soc.* 160 (2013) F923–F930.
- [86] K. Vaarmets, J. Nerut, E. Härk, E. Lust, Electrochemical and physical characterisation of Pt-nanocluster activated molybdenum carbide derived carbon electrodes, *Electrochim. Acta.* 104 (2013) 216–227.
- [87] E. Härk, S. Sepp, P. Valk, K. Vaarmets, J. Nerut, R. Jäger, E. Lust, Impact of the various catalysts (Pt, Pt-Ru) deposited onto carbon support to the slow oxygen reduction reaction kinetics, *ECS Trans.* 45 (2013) 1–11.
- [88] I.N. Leontyev, A.B. Kuriganova, N.G. Leontyev, L. Hennem, A. Rakhmatullin, N.V. Smirnova, V. Dmitriev, Size dependence of the lattice parameters of carbon supported platinum nanoparticles: X-ray diffraction analysis and theoretical considerations, *RSC Adv.* 4 (2014) 35959–35965.
- [89] M.F.C. Ladd, R.A. Palmer, *Structure Determination by X-Ray Crystallography*, Springer, 2003.
- [90] J.U. Keller, R. Staudt, Adsorption isotherms, in: *Gas Adsorpt. Equilibria*, Springer US, 2005: pp. 359–413.
- [91] K.S.W. Sing, Reporting physisorption data for gas/solid systems with special reference to the determination of surface area and porosity (Recommendations 1984), *Pure Appl. Chem.* 57 (1985) 603–619.
- [92] S. Sepp, J. Nerut, K. Vaarmets, R. Kanarbik, E. Härk, E. Lust, The Impact of Pt-Nanocluster Deposition and Nafion® Content on the Oxygen Electroreduction Kinetics on Molybdenum Carbide Derived Carbon Synthesized at 1000° C, *ECS Trans.* 61 (2014) 37–50.
- [93] P. Costamagna, S. Srinivasan, Quantum jumps in the PEMFC science and technology from the 1960s to the year 2000: Part II. Engineering, technology development and application aspects, *J. Power Sources.* 102 (2001) 253–269.
- [94] M. Gara, R.G. Compton, Activity of carbon electrodes towards oxygen reduction in acid: A comparative study, *New J. Chem.* 35 (2011) 2647–2652.

9. SUMMARY IN ESTONIAN

Karbiididest valmistatud süsinikkandjate poorsuse mõju komposiitkatalüsaatorite omadustele madaltemperatuurises kütuseelemendis

Polümeerelektrolüütmembraan (PEM) kütuseelement on seade, mis toodab elektrit kütuse ja oksüdeerija vahelise elektrokeemilise reaktsiooni käigus vabaneva energia arvelt. Kuna PEM kütuseelemendid töötavad võrdlemisi madalal temperatuuril (ca 80 °C), siis on seda võimalik kiiresti käivitada ning kasutada lisaks statsionaarsetele lahendustele ka portatiivsetes rakendustes nagu näiteks elektriauto. PEM kütuseelemendi efektiivsust piirab hapniku elektroredutseerumise reaktsiooni (ORR) suur ülepinge katoodil, seega töötatakse tänapäeval välja palju uudseid katalüsaatorimaterjale, mis seda reaktsiooni kiirendavad.

Enimkasutatud PEM kütuseelemendi elektrodimaterjal on plaatina nanoosakestega aktiveeritud suure eripinnaga süsinik. Antud töös uuriti erinevatest karbiididest sünteetitud süsinikmaterjalide sobivust PEM kütuseelemendi rakenduses ning võrreldi tulemusi kommertsiaalse süsinikmaterjaliga. Erinevate omadustega süsinikmaterjale sünteetiti karbiidide WC ja Mo₂C kõrgtemperatuurise kloreerimise käigus kindlatel temperatuuridel vahemikus 600 kuni 1100 °C. Antud süsinikmaterjalid on kõik suure eripinnaga, kuid erinevad üksteisest kristallilisuse ning pooride suuruse jaotuse poolest.

Süsinikmaterjalidele sadestati plaatina nanoosakesed naatrium-boorhüdriidiga redutseerimise meetodil. Valmistatud süsinike ning platinaga aktiveeritud katalüsaatormaterjalide karakteriseerimiseks kasutati erinevaid füüsikalisi meetodeid: kõrglahutusega skaneeriv elektronmikroskoopia, transmissioelektronmikroskoopia, röntgendifraktsioon, Raman spektroskoopia, lämmastiku sorptsiooni meetod ning termogravimeetria. Nende meetodite abil määrati platinosakeste suurus ning osakaal, materjali kristallilisus ning eripind ja pooride suuruse jaotus. Materjalide elektrokeemiliseks iseloomustamiseks kasutati pöörleva ketaselektroodi, tsüklilise voltamperomeetria, impedantspektroskoopia ja kronopotsiomeetria meetodeid.

ORR kineetikat uuriti kolmeelektroodses süsteemis väävelhappe vesilahuses, kus klaassüsinikust elektroodile oli kantud kas süsinikust katalüsaatorikandja või platinaga aktiveeritud katalüsaatormaterjal. Katalüsaatorikandjana kasutati kaht kõrge eripinnaga karbiidset süsinikku (C(WC) 1100°C ja C(Mo₂C) 800°C), mis erinesid teineteisest grafitiseerituse astme poolest ning samuti testiti kommertsiaalset süsinikku Vulcan XC72. Leiti, et grafitiseerituse astmel (defektide hulgal) ning mikro- ja mesopooride ruumalade suhtel on suur mõju ORRi ülepingele ning uuritud materjalidest oli parim C(Mo₂C) 800°C, mille elektrokeemiline aktiivsus on suurem kui teisel karbiidisel süsinikul C(WC) 1100°C ning oluliselt suurem kommertsiaalse süsiniku Vulcan XC72 aktiivsusest.

Kütuseelemendi membraanelektroodide süsteemi (*membrane electrode assembly*, lühend MEA) valmistamiseks kasutati Mo₂C-st temperatuurivahe-

mikus 600 kuni 1000 °C sünteesitud süsinikmaterjale ning kommertsiaalset süsinikku Vulcan XC72. Tegemaks kindlaks uudsete sünteesitud materjalide sobivust nii kütuseelemendi katoodi kui ka anoodi valmistamiseks, viidi läbi katsed sümmeetriliste (katoodiks ja anoodiks sama uuritav materjal) ja asümmeetriliste (katoodiks uuritav materjal, anoodiks kommertsiaalne Pt-C(Vulcan)) MEAdega. Pt-C(Mo₂C) materjalidest valmistatud MEAd demonstreerisid kütuseelemendis suurimaid võimsustihedusi: kasutades Pt-C(Mo₂C) 800 °C materjali katoodil saavutati maskimaalseks võimsustiheduseks 560 mW cm⁻², kuid samadel tingimustel saavutati kommertsiaalse materjaliga võimsustiheduseks 460 mW cm⁻². Konstantsel voolul läbiviidud stabiilsuse katsed näitasid, et Pt-C(Mo₂C)750 °C materjalist valmistatud kütuseelemendi potentsiaalilangus 0.4 A cm⁻² juures 160 h jooksul oli 240 μV h⁻¹, samas kui kommertsiaalse materjali baasil valmistatud kütuseelemendi vastav näitaja oli 670 μV h⁻¹.

Leiti, et Mo₂C-st sünteesitud süsinikmaterjalid on sobivad katalüsaatori kandjad nii anoodi kui ka katoodi jaoks (sünteesitud vahemikus 600 kuni 850 °C), kuna just nendel materjalidel on lisaks kõrgele eripinnale ka sobilik poorijaotus ning grafitiseerituse aste. Võrreldes laialdaselt kasutatud kommertsiaalse süsinikmaterjaliga on karbiidsete süsinike baasil võimalik valmistada suurema efektiivsusega ning ajalise stabiilsusega PEM kütuseelemente, kuna nende materjalide füüsikalised ning elektrokeemilised omadused on antud rakenduses sobilikumad.

10. ACKNOWLEDGEMENTS

The completion of these thesis has left me indebted to several people to whom I would like to express my gratitude. Thank you, Professor Enn Lust and Jaak Nerut for continuous supervision and encouragement through my scientific work in University of Tartu.

Also I would like to thank Indrek Tallo and Ester Tee for synthesising the CDC powders, Kersti Vaarmets for synthesising catalyst materials, Heisi Kurig and Rasmus Palm for the low temperature N₂ sorption experiments, Rait Kanarbik for HRSEM images, Jaan Aruväli for performing XRD measurements, Jiang Hua from Aalto University for HRTEM measurements.

I am extremely grateful for my friends and family who have always believed in me and motivated me in my chosen path.

This work was supported by the EU through the European Regional Development Fund (projects 2014-2020.4.01.15-0011, 3.2.0101-0030 and 3.2.0302.10-0169), Estonian Target Research Project SF0180002s08 and Institutional Research Grant IUT20-13, Estonian Energy Technology Programme project 3.2.0501.10-0015, Estonian Materials Technology project 3.2.1101.12-0019, Project of European Structure Funds 3.2.0601.11-0001, SLOKT10209T, ESF Grants No. 8865 and 8267, Personal Research Grants PUT55, PUT1033, Graduate Schools “Functional Materials and Technologies” receiving funding from the European Social Fund under project 1.2.0401.09-0079 in Estonia and ASTRA project PER ASPERA Functional Materials and Technologies receiving funding from the European Union Regional Development Fund.

CURRICULUM VITAE

Name: Silver Sepp
Date of birth: April 7, 1987
Citizenship: Estonian
Contact: University of Tartu, Institute of Chemistry
14a Ravila Street, 50411 Tartu, Estonia
E-mail: silver.sepp@ut.ee

Education:

2012–... University of Tartu – Chemistry *Ph.D.* student
2010–2012 University of Tartu – Master’s degree in Materials Science
2006–2010 University of Tartu – Bachelor’s degree in Materials Science
2003–2006 Miina Härma Gymnasium (secondary education)
1994–2003 Puhja Gymnasium (basic education)

Professional employment:

2012–... University of Tartu, Institute of Chemistry, Chemist

List of Publications:

1. S. Sepp, K. Vaarmets, J. Nerut, I. Tallo, E. Tee, H. Kurig; J. Aruväli, R. Kanarbik, E. Lust, Enhanced Activity and Stability of Novel Hierarchical Microporous-Mesoporous Carbon Supports for Polymer Electrolyte Membrane Fuel Cells, *Journal of Solid State Electrochemistry*, (2016) DOI: 10.1007/s10008-016-3448-4.
2. K. Vaarmets, S. Sepp, J. Nerut, E. Lust, Accelerated Durability Tests for Pt-Nanoclusters Modified Carbide Derived Carbons Catalysts in Acidic Solution, *ECS Transactions*, 75(14) (2016) 899–911.
3. S. Sepp, J. Nerut, K. Vaarmets, R. Kanarbik, I. Tallo, H. Kurig, E. Lust, Enhanced Stability of Novel Hierarchical Carbon Supports in PEMFC Application, *ECS Transactions*, 75(14) (2016) 789–799.
4. E. Lust, S. Sepp, J. Nerut, K. Vaarmets, R. Kanarbik, I. Tallo, R. Jäger, E. Härk, P. E. Kasatkin, M. Taleb, Development of Novel Hierarchically Microporous-Mesoporous Carbon and Carbon Nanospheres Based Materials and PEMFC Single Cells, 75(14) (2016) 777–788.
5. S. Sepp, K. Vaarmets, J. Nerut, I. Tallo, E. Tee, H. Kurig; J. Aruväli, R. Kanarbik, E. Lust, Performance of Polymer Electrolyte Membrane Fuel Cell Single Cells Prepared Using Hierarchical Microporous-Mesoporous Carbon Supported Pt Nanoparticles Activated Catalysts, *Electrochimica Acta*, 203 (2016) 221–229.
6. E. Lust, K. Vaarmets, J. Nerut, I. Tallo, P. Valk, S. Sepp, E. Härk, Influence of specific surface area and microporosity-mesoporosity of pristine and Pt-nanoclusters modified carbide derived carbon electrodes on the oxygen electroreduction, *Electrochimica Acta*, 140 (2014) 294–303.

7. S. Sepp, E. Härk, P. Valk, K. Vaarmets, J. Nerut, R. Jäger, E. Lust, Impact of the Pt catalyst on the oxygen electroreduction reaction kinetics on various carbon supports, *Journal of Solid State Electrochemistry*, 18 (5) (2014) 1223–1229.
8. S. Sepp, J. Nerut, K. Vaarmets, R. Kanarbik, I. Tallo, H. Kurig, E. Lust, The Impact of Pt-nanocluster Deposition and Nafion® Content on the Oxygen Electroreduction Kinetics on Molybdenum Carbide Derived Carbon Synthesized at 1000°C, *ECS Transactions* 61 (2014) 37–50
9. E. Härk, V. Steinberg, S. Sepp, K. Vaarmets, J. Nerut, T. Kallio, K. Kontturi, E. Lust, Electrochemical and Physical Characterization of Pt Activated Micromesoporous Vanadium Carbide Derived Carbon Electrodes in Sulfuric Acid Solution, *Journal of the Electrochemical Society*, 160 (9) (2013) F923–F930.
10. K. Vaarmets, S. Sepp, J. Nerut, E. Härk, I. Tallo, E. Lust, Electrochemical and physical characterization of Pt–Ru alloy catalyst deposited onto microporous–mesoporous carbon support derived from Mo₂C at 600 °C, *Journal of Solid State Electrochemistry* 17 (2013) 1729–1741.
11. E. Härk, S. Sepp, P. Valk, K. Vaarmets, J. Nerut, R. Jäger, E. Lust, Impact of the various catalysts (Pt, Pt-Ru) deposited onto carbon support to the slow oxygen reduction reaction kinetics, *ECS Transactions* 45 (2013) 1–11.

Participation in international conferences:

1. S. Sepp, J. Nerut, K. Vaarmets, R. Kanarbik, I. Tallo, H. Kurig, E. Lust, Enhanced Stability of Novel Hierarchical Carbon Supports in PEMFC Application. PRIME 2016, Honolulu, USA, 2–7 Oct. 2016 (oral presentation).
2. S. Sepp, J. Nerut, K. Vaarmets, I. Tallo, H. Kurig, E. Lust, Activity and Stability of Hierarchical Microporous-Mesoporous Carbon Supported Pt-Catalysts in PEMFC Application. 18th Topical Meeting of ISE, Gwangju, South Korea, 8–11 March 2016 (poster presentation).
3. S. Sepp, J. Nerut, K. Vaarmets, I. Tallo, H. Kurig, E. Lust, Performance of PEMFC Half Cells Prepared Using Hierarchical Microporous-Macroporous Carbon Supported Pt-Catalyst. 66th Annual Meeting of ISE, Taipei, Taiwan, 4–9 Oct. 2015 (oral presentation).
4. S. Sepp, J. Nerut, E. Härk, K. Vaarmets, I. Tallo, E. Tee, A. Jänes, E. Lust, Oxygen Electroreduction Studied on Carbon Materials Synthesized from SiC and Post-Activated with Reactive Gases. 65th Annual Meeting of ISE, Lausanne, Switzerland, 31 Aug. – 5 Sept. 2014 (poster presentation).
5. S. Sepp, J. Nerut, K. Vaarmets, R. Kanarbik, E. Härk, E. Lust, The Impact of Pt-nanocluster Deposition and Nafion® Content on ORR on Molybdenum Carbide Derived Carbon Synthesized at 1000°C. 225th ECS Meeting; Orlando, USA, 11–15 May 2014 (poster presentation).
6. S. Sepp, J. Nerut, E. Härk, K. Vaarmets, P. Valk, E. Lust, Activity of Various Carbide Derived Carbons Towards Oxygen Electroreduction in Acidic

- Solutions. 64th Annual Meeting of ISE, Queretaro, Mexico, 8–13 Sept. 2013 (oral presentation).
7. E. Härk, S. Sepp, P. Valk, K. Vaarmets, J. Nerut, R. Jäger, E. Lust, Impact of the Various Catalysts (Pt, Pt-Ru) Deposited onto Carbon Support to the Slow Oxygen Reduction Reaction Kinetics. 221st ECS Meeting, Seattle, USA, 6–10 May 2012 (oral presentation).

ELULOOKIRJELDUS

Nimi: Silver Sepp
Sünniaeg: 7. aprill 1987
Kodakondsus: Eesti
Kontakt: Tartu Ülikooli keemia instituut
Ravila 14A, 50411 Tartu, Eesti
E-mail: silver.sepp@ut.ee

Haridus:
2012–... Tartu Ülikool – keemia doktorant
2010–2012 Tartu Ülikool – magistrikraad materjaliteaduses
2006–2010 Tartu Ülikool – bakalaureusekraad materjaliteaduses
2003–2006 Miina Härma Gümnaasium (keskharudus)
1994–2003 Puhja Gümnaasium (põhiharudus)

Töökogemus:
2012–... Tartu Ülikooli keemia instituut, keemik

Teaduspublikatsioonid:

1. S. Sepp, K. Vaarmets, J. Nerut, I. Tallo, E. Tee, H. Kurig; J. Aruväli, R. Kanarbik, E. Lust, Enhanced Activity and Stability of Novel Hierarchical Microporous-Mesoporous Carbon Supports for Polymer Electrolyte Membrane Fuel Cells, *Journal of Solid State Electrochemistry*, (2016) DOI: 10.1007/s10008-016-3448-4
2. K. Vaarmets, S. Sepp, J. Nerut, E. Lust, Accelerated Durability Tests for Pt -Nanoclusters Modified Carbide Derived Carbons Catalysts in Acidic Solution, *ECS Transactions*, 75(14) (2016) 899–911.
3. S. Sepp, J. Nerut, K. Vaarmets, R. Kanarbik, I. Tallo, H. Kurig, E. Lust, Enhanced Stability of Novel Hierarchical Carbon Supports in PEMFC Application, *ECS Transactions*, 75(14) (2016) 789–799.
4. E. Lust, S. Sepp, J. Nerut, K. Vaarmets, R. Kanarbik, I. Tallo, R. Jäger, E. Härk, P. E. Kasatkin, M. Taleb, Development of Novel Hierarchically Microporous-Mesoporous Carbon and Carbon Nanospheres Based Materials and PEMFC Single Cells, 75(14) (2016) 777–788.
5. S. Sepp, K. Vaarmets, J. Nerut, I. Tallo, E. Tee, H. Kurig; J. Aruväli, R. Kanarbik, E. Lust, Performance of Polymer Electrolyte Membrane Fuel Cell Single Cells Prepared Using Hierarchical Microporous-Mesoporous Carbon Supported Pt Nanoparticles Activated Catalysts, *Electrochimica Acta*, 203 (2016) 221–229.
6. E. Lust, K. Vaarmets, J. Nerut, I. Tallo, P. Valk, S. Sepp, E. Härk, Influence of specific surface area and microporosity-mesoporosity of pristine and Pt-nanoclusters modified carbide derived carbon electrodes on the oxygen electroreduction, *Electrochimica Acta*, 140 (2014) 294–303.

7. S. Sepp, E. Härk, P. Valk, K. Vaarmets, J. Nerut, R. Jäger, E. Lust, Impact of the Pt catalyst on the oxygen electroreduction reaction kinetics on various carbon supports, *Journal of Solid State Electrochemistry*, 18 (5) (2014) 1223–1229.
8. S. Sepp, J. Nerut, K. Vaarmets, R. Kanarbik, I. Tallo, H. Kurig, E. Lust, The Impact of Pt-nanocluster Deposition and Nafion® Content on the Oxygen Electroreduction Kinetics on Molybdenum Carbide Derived Carbon Synthesized at 1000°C, *ECS Transactions* 61 (2014) 37–50
9. E. Härk, V. Steinberg, S. Sepp, K. Vaarmets, J. Nerut, T. Kallio, K. Kontturi, E. Lust, Electrochemical and Physical Characterization of Pt Activated Micromesoporous Vanadium Carbide Derived Carbon Electrodes in Sulfuric Acid Solution, *Journal of the Electrochemical Society*, 160 (9) (2013) F923–F930.
10. K. Vaarmets, S. Sepp, J. Nerut, E. Härk, I. Tallo, E. Lust, Electrochemical and physical characterization of Pt–Ru alloy catalyst deposited onto microporous–mesoporous carbon support derived from Mo₂C at 600 °C, *Journal of Solid State Electrochemistry* 17 (2013) 1729–1741.
11. E. Härk, S. Sepp, P. Valk, K. Vaarmets, J. Nerut, R. Jäger, E. Lust, Impact of the various catalysts (Pt, Pt-Ru) deposited onto carbon support to the slow oxygen reduction reaction kinetics, *ECS Transactions* 45 (2013) 1–11.

Rahvusvahelistel konverentsidel osalemine:

1. S. Sepp, J. Nerut, K. Vaarmets, R. Kanarbik, I. Tallo, H. Kurig, E. Lust, Enhanced Stability of Novel Hierarchical Carbon Supports in PEMFC Application. PRIME 2016, Honolulu, USA, 2.10.16–7.10.16 (suuline ettekanne).
2. S. Sepp, J. Nerut, K. Vaarmets, I. Tallo, H. Kurig, E. Lust, Activity and Stability of Hierarchical Microporous-Mesoporous Carbon Supported Pt-Catalysts in PEMFC Application. 18th Topical Meeting of ISE, Gwangju, Lõuna-Korea, 8.03.16–11.03.16 (posterettekanne).
3. S. Sepp, J. Nerut, K. Vaarmets, I. Tallo, H. Kurig, E. Lust, Performance of PEMFC Half Cells Prepared Using Hierarchical Microporous-Macroporous Carbon Supported Pt-Catalyst. 66th Annual Meeting of ISE, Taipei, Taiwan, 4.10.15–9.10.15 (suuline ettekanne).
4. S. Sepp, J. Nerut, E. Härk, K. Vaarmets, I. Tallo, E. Tee, A. Jänes, E. Lust, Oxygen Electroreduction Studied on Carbon Materials Synthesized from SiC and Post-Activated with Reactive Gases. 65th Annual Meeting of ISE, Lausanne, Šveits, 31.08.14–5.09.14 (posterettekanne).
5. S. Sepp, J. Nerut, K. Vaarmets, R. Kanarbik, E. Härk, E. Lust, The Impact of Pt-nanocluster Deposition and Nafion® Content on ORR on Molybdenum Carbide Derived Carbon Synthesized at 1000°C. 225th ECS Meeting; Orlando, USA, 11.05.14–15.05.14 (posterettekanne).
6. S. Sepp, J. Nerut, E. Härk, K. Vaarmets, P. Valk, E. Lust, Activity of Various Carbide Derived Carbons Towards Oxygen Electroreduction in Acidic

- Solutions. 64th Annual Meeting of ISE, Queretaro, Mehiko, 8.09.13–13.09.13 (suuline ettekanne).
7. E. Härk, S. Sepp, P. Valk, K. Vaarmets, J. Nerut, R. Jäger, E. Lust, Impact of the Various Catalysts (Pt, Pt-Ru) Deposited onto Carbon Support to the Slow Oxygen Reduction Reaction Kinetics. 221st ECS Meeting, Seattle, USA, 6.05.12–10.05.12 (suuline ettekanne).

DISSERTATIONES CHIMICAE UNIVERSITATIS TARTUENSIS

1. **Toomas Tamm.** Quantum-chemical simulation of solvent effects. Tartu, 1993, 110 p.
2. **Peeter Burk.** Theoretical study of gas-phase acid-base equilibria. Tartu, 1994, 96 p.
3. **Victor Lobanov.** Quantitative structure-property relationships in large descriptor spaces. Tartu, 1995, 135 p.
4. **Vahur Mäemets.** The ^{17}O and ^1H nuclear magnetic resonance study of H_2O in individual solvents and its charged clusters in aqueous solutions of electrolytes. Tartu, 1997, 140 p.
5. **Andrus Metsala.** Microcanonical rate constant in nonequilibrium distribution of vibrational energy and in restricted intramolecular vibrational energy redistribution on the basis of Slater's theory of unimolecular reactions. Tartu, 1997, 150 p.
6. **Uko Maran.** Quantum-mechanical study of potential energy surfaces in different environments. Tartu, 1997, 137 p.
7. **Alar Jänes.** Adsorption of organic compounds on antimony, bismuth and cadmium electrodes. Tartu, 1998, 219 p.
8. **Kaido Tammeveski.** Oxygen electroreduction on thin platinum films and the electrochemical detection of superoxide anion. Tartu, 1998, 139 p.
9. **Ivo Leito.** Studies of Brønsted acid-base equilibria in water and non-aqueous media. Tartu, 1998, 101 p.
10. **Jaan Leis.** Conformational dynamics and equilibria in amides. Tartu, 1998, 131 p.
11. **Toonika Rincken.** The modelling of amperometric biosensors based on oxidoreductases. Tartu, 2000, 108 p.
12. **Dmitri Panov.** Partially solvated Grignard reagents. Tartu, 2000, 64 p.
13. **Kaja Orupõld.** Treatment and analysis of phenolic wastewater with microorganisms. Tartu, 2000, 123 p.
14. **Jüri Ivask.** Ion Chromatographic determination of major anions and cations in polar ice core. Tartu, 2000, 85 p.
15. **Lauri Vares.** Stereoselective Synthesis of Tetrahydrofuran and Tetrahydropyran Derivatives by Use of Asymmetric Horner-Wadsworth-Emmons and Ring Closure Reactions. Tartu, 2000, 184 p.
16. **Martin Lepiku.** Kinetic aspects of dopamine D_2 receptor interactions with specific ligands. Tartu, 2000, 81 p.
17. **Katrin Sak.** Some aspects of ligand specificity of P2Y receptors. Tartu, 2000, 106 p.
18. **Vello Pällin.** The role of solvation in the formation of iotsitch complexes. Tartu, 2001, 95 p.
19. **Katrin Kollist.** Interactions between polycyclic aromatic compounds and humic substances. Tartu, 2001, 93 p.

20. **Ivar Koppel.** Quantum chemical study of acidity of strong and superstrong Brønsted acids. Tartu, 2001, 104 p.
21. **Viljar Pihl.** The study of the substituent and solvent effects on the acidity of OH and CH acids. Tartu, 2001, 132 p.
22. **Natalia Palm.** Specification of the minimum, sufficient and significant set of descriptors for general description of solvent effects. Tartu, 2001, 134 p.
23. **Sulev Sild.** QSPR/QSAR approaches for complex molecular systems. Tartu, 2001, 134 p.
24. **Ruslan Petrukhin.** Industrial applications of the quantitative structure-property relationships. Tartu, 2001, 162 p.
25. **Boris V. Rogovoy.** Synthesis of (benzotriazolyl)carboximidamides and their application in relations with *N*- and *S*-nucleophyles. Tartu, 2002, 84 p.
26. **Koit Herodes.** Solvent effects on UV-vis absorption spectra of some solvatochromic substances in binary solvent mixtures: the preferential solvation model. Tartu, 2002, 102 p.
27. **Anti Perkson.** Synthesis and characterisation of nanostructured carbon. Tartu, 2002, 152 p.
28. **Ivari Kaljurand.** Self-consistent acidity scales of neutral and cationic Brønsted acids in acetonitrile and tetrahydrofuran. Tartu, 2003, 108 p.
29. **Karmen Lust.** Adsorption of anions on bismuth single crystal electrodes. Tartu, 2003, 128 p.
30. **Mare Piirsalu.** Substituent, temperature and solvent effects on the alkaline hydrolysis of substituted phenyl and alkyl esters of benzoic acid. Tartu, 2003, 156 p.
31. **Meeri Sassian.** Reactions of partially solvated Grignard reagents. Tartu, 2003, 78 p.
32. **Tarmo Tamm.** Quantum chemical modelling of polypyrrole. Tartu, 2003. 100 p.
33. **Erik Teinmaa.** The environmental fate of the particulate matter and organic pollutants from an oil shale power plant. Tartu, 2003. 102 p.
34. **Jaana Tammiku-Taul.** Quantum chemical study of the properties of Grignard reagents. Tartu, 2003. 120 p.
35. **Andre Lomaka.** Biomedical applications of predictive computational chemistry. Tartu, 2003. 132 p.
36. **Kostyantyn Kirichenko.** Benzotriazole – Mediated Carbon–Carbon Bond Formation. Tartu, 2003. 132 p.
37. **Gunnar Nurk.** Adsorption kinetics of some organic compounds on bismuth single crystal electrodes. Tartu, 2003, 170 p.
38. **Mati Arulepp.** Electrochemical characteristics of porous carbon materials and electrical double layer capacitors. Tartu, 2003, 196 p.
39. **Dan Cornel Fara.** QSPR modeling of complexation and distribution of organic compounds. Tartu, 2004, 126 p.
40. **Riina Mahlapuu.** Signalling of galanin and amyloid precursor protein through adenylate cyclase. Tartu, 2004, 124 p.

41. **Mihkel Kerikmäe.** Some luminescent materials for dosimetric applications and physical research. Tartu, 2004, 143 p.
42. **Jaanus Kruusma.** Determination of some important trace metal ions in human blood. Tartu, 2004, 115 p.
43. **Urmas Johanson.** Investigations of the electrochemical properties of polypyrrole modified electrodes. Tartu, 2004, 91 p.
44. **Kaido Sillar.** Computational study of the acid sites in zeolite ZSM-5. Tartu, 2004, 80 p.
45. **Aldo Oras.** Kinetic aspects of dATP α S interaction with P2Y₁ receptor. Tartu, 2004, 75 p.
46. **Erik Mölder.** Measurement of the oxygen mass transfer through the air-water interface. Tartu, 2005, 73 p.
47. **Thomas Thomberg.** The kinetics of electroreduction of peroxodisulfate anion on cadmium (0001) single crystal electrode. Tartu, 2005, 95 p.
48. **Olavi Loog.** Aspects of condensations of carbonyl compounds and their imine analogues. Tartu, 2005, 83 p.
49. **Siim Salmar.** Effect of ultrasound on ester hydrolysis in aqueous ethanol. Tartu, 2006, 73 p.
50. **Ain Uustare.** Modulation of signal transduction of heptahelical receptors by other receptors and G proteins. Tartu, 2006, 121 p.
51. **Sergei Yurchenko.** Determination of some carcinogenic contaminants in food. Tartu, 2006, 143 p.
52. **Kaido Tamm.** QSPR modeling of some properties of organic compounds. Tartu, 2006, 67 p.
53. **Olga Tšubrik.** New methods in the synthesis of multisubstituted hydrazines. Tartu, 2006, 183 p.
54. **Lilli Sooväli.** Spectrophotometric measurements and their uncertainty in chemical analysis and dissociation constant measurements. Tartu, 2006, 125 p.
55. **Eve Koort.** Uncertainty estimation of potentiometrically measured pH and pK_a values. Tartu, 2006, 139 p.
56. **Sergei Kopanchuk.** Regulation of ligand binding to melanocortin receptor subtypes. Tartu, 2006, 119 p.
57. **Silvar Kallip.** Surface structure of some bismuth and antimony single crystal electrodes. Tartu, 2006, 107 p.
58. **Kristjan Saal.** Surface silanization and its application in biomolecule coupling. Tartu, 2006, 77 p.
59. **Tanel Tätte.** High viscosity Sn(OBu)₄ oligomeric concentrates and their applications in technology. Tartu, 2006, 91 p.
60. **Dimitar Atanasov Dobchev.** Robust QSAR methods for the prediction of properties from molecular structure. Tartu, 2006, 118 p.
61. **Hannes Hagu.** Impact of ultrasound on hydrophobic interactions in solutions. Tartu, 2007, 81 p.

62. **Rutha Jäger.** Electroreduction of peroxodisulfate anion on bismuth electrodes. Tartu, 2007, 142 p.
63. **Kaido Viht.** Immobilizable bisubstrate-analogue inhibitors of basophilic protein kinases: development and application in biosensors. Tartu, 2007, 88 p.
64. **Eva-Ingrid Rõõm.** Acid-base equilibria in nonpolar media. Tartu, 2007, 156 p.
65. **Sven Tamp.** DFT study of the cesium cation containing complexes relevant to the cesium cation binding by the humic acids. Tartu, 2007, 102 p.
66. **Jaak Nerut.** Electroreduction of hexacyanoferrate(III) anion on Cadmium (0001) single crystal electrode. Tartu, 2007, 180 p.
67. **Lauri Jalukse.** Measurement uncertainty estimation in amperometric dissolved oxygen concentration measurement. Tartu, 2007, 112 p.
68. **Aime Lust.** Charge state of dopants and ordered clusters formation in CaF₂:Mn and CaF₂:Eu luminophors. Tartu, 2007, 100 p.
69. **Iiris Kahn.** Quantitative Structure-Activity Relationships of environmentally relevant properties. Tartu, 2007, 98 p.
70. **Mari Reinik.** Nitrates, nitrites, N-nitrosamines and polycyclic aromatic hydrocarbons in food: analytical methods, occurrence and dietary intake. Tartu, 2007, 172 p.
71. **Heili Kasuk.** Thermodynamic parameters and adsorption kinetics of organic compounds forming the compact adsorption layer at Bi single crystal electrodes. Tartu, 2007, 212 p.
72. **Erki Enkvist.** Synthesis of adenosine-peptide conjugates for biological applications. Tartu, 2007, 114 p.
73. **Svetoslav Hristov Slavov.** Biomedical applications of the QSAR approach. Tartu, 2007, 146 p.
74. **Eneli Härk.** Electroreduction of complex cations on electrochemically polished Bi(*hkl*) single crystal electrodes. Tartu, 2008, 158 p.
75. **Priit Möller.** Electrochemical characteristics of some cathodes for medium temperature solid oxide fuel cells, synthesized by solid state reaction technique. Tartu, 2008, 90 p.
76. **Signe Viggor.** Impact of biochemical parameters of genetically different pseudomonads at the degradation of phenolic compounds. Tartu, 2008, 122 p.
77. **Ave Sarapuu.** Electrochemical reduction of oxygen on quinone-modified carbon electrodes and on thin films of platinum and gold. Tartu, 2008, 134 p.
78. **Agnes Kütt.** Studies of acid-base equilibria in non-aqueous media. Tartu, 2008, 198 p.
79. **Rouvim Kadis.** Evaluation of measurement uncertainty in analytical chemistry: related concepts and some points of misinterpretation. Tartu, 2008, 118 p.
80. **Valter Reedo.** Elaboration of IVB group metal oxide structures and their possible applications. Tartu, 2008, 98 p.

81. **Aleksei Kuznetsov.** Allosteric effects in reactions catalyzed by the cAMP-dependent protein kinase catalytic subunit. Tartu, 2009, 133 p.
82. **Aleksei Bredihhin.** Use of mono- and polyanions in the synthesis of multisubstituted hydrazine derivatives. Tartu, 2009, 105 p.
83. **Anu Ploom.** Quantitative structure-reactivity analysis in organosilicon chemistry. Tartu, 2009, 99 p.
84. **Argo Vonk.** Determination of adenosine A_{2A}- and dopamine D₁ receptor-specific modulation of adenylate cyclase activity in rat striatum. Tartu, 2009, 129 p.
85. **Indrek Kivi.** Synthesis and electrochemical characterization of porous cathode materials for intermediate temperature solid oxide fuel cells. Tartu, 2009, 177 p.
86. **Jaanus Eskusson.** Synthesis and characterisation of diamond-like carbon thin films prepared by pulsed laser deposition method. Tartu, 2009, 117 p.
87. **Marko Lätt.** Carbide derived microporous carbon and electrical double layer capacitors. Tartu, 2009, 107 p.
88. **Vladimir Stepanov.** Slow conformational changes in dopamine transporter interaction with its ligands. Tartu, 2009, 103 p.
89. **Aleksander Trummal.** Computational Study of Structural and Solvent Effects on Acidities of Some Brønsted Acids. Tartu, 2009, 103 p.
90. **Eerold Vellemäe.** Applications of mischmetal in organic synthesis. Tartu, 2009, 93 p.
91. **Sven Parkel.** Ligand binding to 5-HT_{1A} receptors and its regulation by Mg²⁺ and Mn²⁺. Tartu, 2010, 99 p.
92. **Signe Vahur.** Expanding the possibilities of ATR-FT-IR spectroscopy in determination of inorganic pigments. Tartu, 2010, 184 p.
93. **Tavo Romann.** Preparation and surface modification of bismuth thin film, porous, and microelectrodes. Tartu, 2010, 155 p.
94. **Nadežda Aleksejeva.** Electrocatalytic reduction of oxygen on carbon nanotube-based nanocomposite materials. Tartu, 2010, 147 p.
95. **Marko Kullapere.** Electrochemical properties of glassy carbon, nickel and gold electrodes modified with aryl groups. Tartu, 2010, 233 p.
96. **Liis Siinor.** Adsorption kinetics of ions at Bi single crystal planes from aqueous electrolyte solutions and room-temperature ionic liquids. Tartu, 2010, 101 p.
97. **Angela Vaasa.** Development of fluorescence-based kinetic and binding assays for characterization of protein kinases and their inhibitors. Tartu 2010, 101 p.
98. **Indrek Tulp.** Multivariate analysis of chemical and biological properties. Tartu 2010, 105 p.
99. **Aare Selberg.** Evaluation of environmental quality in Northern Estonia by the analysis of leachate. Tartu 2010, 117 p.
100. **Darja Lavõgina.** Development of protein kinase inhibitors based on adenosine analogue-oligoarginine conjugates. Tartu 2010, 248 p.

101. **Laura Herm.** Biochemistry of dopamine D₂ receptors and its association with motivated behaviour. Tartu 2010, 156 p.
102. **Terje Raudsepp.** Influence of dopant anions on the electrochemical properties of polypyrrole films. Tartu 2010, 112 p.
103. **Margus Marandi.** Electroformation of Polypyrrole Films: *In-situ* AFM and STM Study. Tartu 2011, 116 p.
104. **Kairi Kivirand.** Diamine oxidase-based biosensors: construction and working principles. Tartu, 2011, 140 p.
105. **Anneli Kruve.** Matrix effects in liquid-chromatography electrospray mass-spectrometry. Tartu, 2011, 156 p.
106. **Gary Urb.** Assessment of environmental impact of oil shale fly ash from PF and CFB combustion. Tartu, 2011, 108 p.
107. **Nikita Oskolkov.** A novel strategy for peptide-mediated cellular delivery and induction of endosomal escape. Tartu, 2011, 106 p.
108. **Dana Martin.** The QSPR/QSAR approach for the prediction of properties of fullerene derivatives. Tartu, 2011, 98 p.
109. **Säde Viirlaid.** Novel glutathione analogues and their antioxidant activity. Tartu, 2011, 106 p.
110. **Ülis Sõukand.** Simultaneous adsorption of Cd²⁺, Ni²⁺, and Pb²⁺ on peat. Tartu, 2011, 124 p.
111. **Lauri Lipping.** The acidity of strong and superstrong Brønsted acids, an outreach for the “limits of growth”: a quantum chemical study. Tartu, 2011, 124 p.
112. **Heisi Kurig.** Electrical double-layer capacitors based on ionic liquids as electrolytes. Tartu, 2011, 146 p.
113. **Marje Kasari.** Bisubstrate luminescent probes, optical sensors and affinity adsorbents for measurement of active protein kinases in biological samples. Tartu, 2012, 126 p.
114. **Kalev Takkis.** Virtual screening of chemical databases for bioactive molecules. Tartu, 2012, 122 p.
115. **Ksenija Kisseljova.** Synthesis of aza-β³-amino acid containing peptides and kinetic study of their phosphorylation by protein kinase A. Tartu, 2012, 104 p.
116. **Riin Rebane.** Advanced method development strategy for derivatization LC/ESI/MS. Tartu, 2012, 184 p.
117. **Vladislav Ivaništšev.** Double layer structure and adsorption kinetics of ions at metal electrodes in room temperature ionic liquids. Tartu, 2012, 128 p.
118. **Irja Helm.** High accuracy gravimetric Winkler method for determination of dissolved oxygen. Tartu, 2012, 139 p.
119. **Karin Kipper.** Fluoroalcohols as Components of LC-ESI-MS Eluents: Usage and Applications. Tartu, 2012, 164 p.
120. **Arno Ratas.** Energy storage and transfer in dosimetric luminescent materials. Tartu, 2012, 163 p.

121. **Reet Reinart-Okugbeni.** Assay systems for characterisation of subtype-selective binding and functional activity of ligands on dopamine receptors. Tartu, 2012, 159 p.
122. **Lauri Sikk.** Computational study of the Sonogashira cross-coupling reaction. Tartu, 2012, 81 p.
123. **Karita Raudkivi.** Neurochemical studies on inter-individual differences in affect-related behaviour of the laboratory rat. Tartu, 2012, 161 p.
124. **Indrek Saar.** Design of GalR2 subtype specific ligands: their role in depression-like behavior and feeding regulation. Tartu, 2013, 126 p.
125. **Ann Laheäär.** Electrochemical characterization of alkali metal salt based non-aqueous electrolytes for supercapacitors. Tartu, 2013, 127 p.
126. **Kerli Tõnurist.** Influence of electrospun separator materials properties on electrochemical performance of electrical double-layer capacitors. Tartu, 2013, 147 p.
127. **Kaija Põhako-Esko.** Novel organic and inorganic ionogels: preparation and characterization. Tartu, 2013, 124 p.
128. **Ivar Kruusenberg.** Electroreduction of oxygen on carbon nanomaterial-based catalysts. Tartu, 2013, 191 p.
129. **Sander Piiskop.** Kinetic effects of ultrasound in aqueous acetonitrile solutions. Tartu, 2013, 95 p.
130. **Iлона Faustova.** Regulatory role of L-type pyruvate kinase N-terminal domain. Tartu, 2013, 109 p.
131. **Kadi Tamm.** Synthesis and characterization of the micro-mesoporous anode materials and testing of the medium temperature solid oxide fuel cell single cells. Tartu, 2013, 138 p.
132. **Iva Bozhidarova Stoyanova-Slavova.** Validation of QSAR/QSPR for regulatory purposes. Tartu, 2013, 109 p.
133. **Vitali Grozovski.** Adsorption of organic molecules at single crystal electrodes studied by *in situ* STM method. Tartu, 2014, 146 p.
134. **Santa Veikšina.** Development of assay systems for characterisation of ligand binding properties to melanocortin 4 receptors. Tartu, 2014, 151 p.
135. **Jüri Liiv.** PVDF (polyvinylidene difluoride) as material for active element of twisting-ball displays. Tartu, 2014, 111 p.
136. **Kersti Vaarmets.** Electrochemical and physical characterization of pristine and activated molybdenum carbide-derived carbon electrodes for the oxygen electroreduction reaction. Tartu, 2014, 131 p.
137. **Lauri Tõntson.** Regulation of G-protein subtypes by receptors, guanine nucleotides and Mn²⁺. Tartu, 2014, 105 p.
138. **Aiko Adamson.** Properties of amine-boranes and phosphorus analogues in the gas phase. Tartu, 2014, 78 p.
139. **Elo Kibena.** Electrochemical grafting of glassy carbon, gold, highly oriented pyrolytic graphite and chemical vapour deposition-grown graphene electrodes by diazonium reduction method. Tartu, 2014, 184 p.

140. **Teemu Näykki.** Novel Tools for Water Quality Monitoring – From Field to Laboratory. Tartu, 2014, 202 p.
141. **Karl Kaupmees.** Acidity and basicity in non-aqueous media: importance of solvent properties and purity. Tartu, 2014, 128 p.
142. **Oleg Lebedev.** Hydrazine polyanions: different strategies in the synthesis of heterocycles. Tartu, 2015, 118 p.
143. **Geven Piir.** Environmental risk assessment of chemicals using QSAR methods. Tartu, 2015, 123 p.
144. **Olga Mazina.** Development and application of the biosensor assay for measurements of cyclic adenosine monophosphate in studies of G protein-coupled receptor signaling. Tartu, 2015, 116 p.
145. **Sandip Ashokrao Kadam.** Anion receptors: synthesis and accurate binding measurements. Tartu, 2015, 116 p.
146. **Indrek Tallo.** Synthesis and characterization of new micro-mesoporous carbide derived carbon materials for high energy and power density electrical double layer capacitors. Tartu, 2015, 148 p.
147. **Heiki Erikson.** Electrochemical reduction of oxygen on nanostructured palladium and gold catalysts. Tartu, 2015, 204 p.
148. **Erik Anderson.** *In situ* Scanning Tunnelling Microscopy studies of the interfacial structure between Bi(111) electrode and a room temperature ionic liquid. Tartu, 2015, 118 p.
149. **Girinath G. Pillai.** Computational Modelling of Diverse Chemical, Biochemical and Biomedical Properties. Tartu, 2015, 140 p.
150. **Piret Pikma.** Interfacial structure and adsorption of organic compounds at Cd(0001) and Sb(111) electrodes from ionic liquid and aqueous electrolytes: an *in situ* STM study. Tartu, 2015, 126 p.
151. **Ganesh babu Manoharan.** Combining chemical and genetic approaches for photoluminescence assays of protein kinases. Tartu, 2016, 126 p.
152. **Carolyn Siimenson.** Electrochemical characterization of halide ion adsorption from liquid mixtures at Bi(111) and pyrolytic graphite electrode surface. Tartu, 2016, 110 p.
153. **Asko Laaniste.** Comparison and optimisation of novel mass spectrometry ionisation sources. Tartu, 2016, 156 p.
154. **Hanno Evard.** Estimating limit of detection for mass spectrometric analysis methods. Tartu, 2016, 224 p.
155. **Kadri Ligi.** Characterization and application of protein kinase-responsive organic probes with triplet-singlet energy transfer. Tartu, 2016, 122 p.
156. **Margarita Kagan.** Biosensing penicillins' residues in milk flows. Tartu, 2016, 130 p.
157. **Marie Kriisa.** Development of protein kinase-responsive photoluminescent probes and cellular regulators of protein phosphorylation. Tartu, 2016, 106 p.
158. **Mihkel Vestli.** Ultrasonic spray pyrolysis deposited electrolyte layers for intermediate temperature solid oxide fuel cells. Tartu 2016, 156 p.